Acta Societatis Botanicorum Poloniae

DOI: 10.5586/asbp.3533

Publication history
Received: 2016-12-01
Accepted: 2016-12-31
Published: 2016-12-31

Handling editors
Beata Zagórska-Marek, Faculty of Biological Sciences, University of Wrocław, Poland
Przemysław Prusinkiewicz, Faculty of Science, University of Calgary, Canada

Authors' contributions
CG wrote the programs and ran the simulations; SD wrote one program and one simulation; CG and SD analyzed the results; CG, JD, and SD wrote the article

Funding
This work was supported in part by a National Science Foundation (NSF) collaborative grant 0540740 to CG and an NSF collaborative grant 0540662 to JD.

Competing interests
No competing interests have been declared.

Citation
Golé C, Dumais J, Douady S. Fibonacci or quasi-symmetric phyllotaxis. Part I: why? Acta Soc Bot Pol. 2016;85(4):3533. https://doi.org/10.5586/asbp.3533

INVITED ORIGINAL RESEARCH PAPER

Fibonacci or quasi-symmetric phyllotaxis. Part I: why?

Christophe Golé[1]*, Jacques Dumais[2], Stéphane Douady[3]

[1] Department of Mathematics, Smith College, Northampton, MA 01063, USA
[2] Faculty of Engineering and Sciences, Universidad Adolfo Ibáñez, Viña del Mar, Chile
[3] UMR 7057 Université Paris Diderot – CNRS, Bâtiment Condorcet, CC 7057, 10 rue Alice Domon et Léonie Duquet, 75013 Paris, France

* Corresponding author. Email: cgole@smith.edu

Abstract
The study of phyllotaxis has focused on seeking explanations for the occurrence of consecutive Fibonacci numbers in the number of helices paving the stems of plants in the two opposite directions. Using the disk-accretion model, first introduced by Schwendener and justified by modern biological studies, we observe two distinct types of solutions: the classical Fibonacci-like ones, and also more irregular configurations exhibiting nearly equal number of helices in a quasi-square packing, the quasi-symmetric ones, which are a generalization of the whorled patterns. Defining new geometric tools allowing to work with irregular patterns and local transitions, we provide simple explanations for the emergence of these two states within the same elementary model. A companion paper will provide a wide array of plant data analyses that support our view.

Keywords
phyllotaxis; Fibonacci; quasi-symmetry; disc-stacking model; irregular pattern

Introduction

Phyllotaxis is the arrangement of lateral organs in plants [1]. This arrangement can be surprisingly regular, revealing two families of spirals or helices, called parastichies, crisscrossing to form lattice-like patterns (Fig. 1). The number of parastichies in both families is often a pair of successive Fibonacci numbers, namely 1, 1, 2, 3, 5, 8, … . Many other patterns have also been observed. For instance, those with parastichy numbers in the Lucas sequence 1, 3, 4, 7, 11, … built recursively by adding the last two terms to obtain the next, as for the Fibonacci sequence, but with a different pair of initial terms. Another kind of pattern, the whorled patterns, where n primordia appear at the same level on the stem, form equal numbers (n, n) of parastichies. These whorled patterns can themselves give rise to Fibonacci-like patterns, the so-called multijugate patterns, with starting point (n, n) instead of (1, 1). The most common is the bijugate pattern, with parastichy numbers in the sequence 2, 2, 4, 6, 10, 16, …, the Fibonacci sequence with each term multiplied by 2.

The central problem of phyllotaxis is to explain the origin of these patterns. Putative explanations abound and range from purely geometrical arguments [1–7] to detailed simulations of the diffusion and interaction of various molecular species at the shoot apical meristem [8–15]. However, fewer investigations offer a clear statement of the conditions necessary to achieve specific phyllotactic patterns. We tackle this challenge with the simplest possible model of phyllotaxis. This approach not only has allowed us to provide a simple explanation for the dominance of Fibonacci-like patterns in plants but it also helped us establish the existence of another mostly ignored kind of phyllotactic pattern, the quasi-symmetric patterns. Quasi-symmetric patterns are those where the parastichy numbers do not follow a Fibonacci recurrence, but

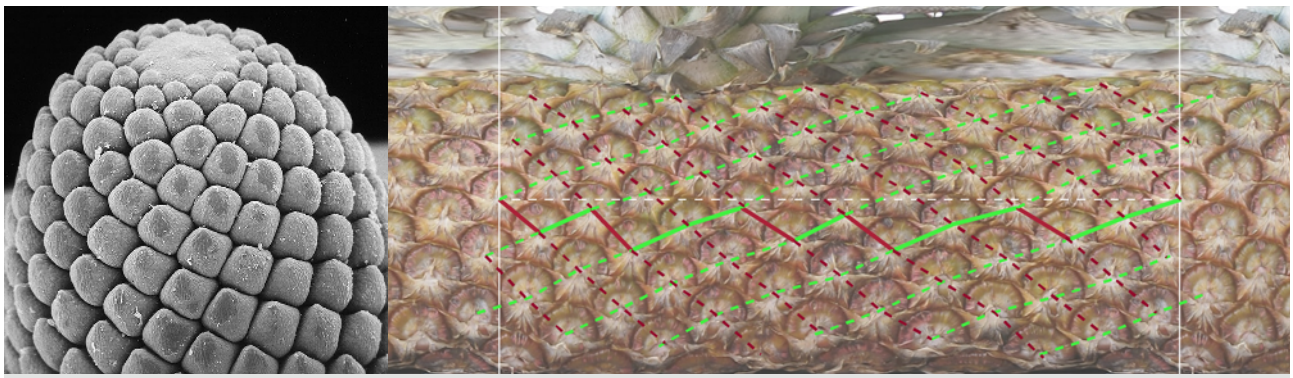

Fig. 1 Primordia and parastichies. Left (courtesy R. Rutishauer): micrograph of a *Picea* sp. branch tip. The zone of formation of the primordia is seen on the edge of the bare zone, the meristem. As the branch grows, new primordia are left behind, forming parastichies. Right: unrolled pineapple. The vertical lines represent the boundaries of a full turn. This pineapple has a (5, 8) pattern: five green parastichies in the direction NE to SW, and eight red ones in the direction NW to SE. A zigzagging front is shown in bold. It is the highest layer of scales lower than the white dashed line, representing the latest primordia at at given instant of growth. The number (three here) of red parastichies is equal to the number of green vectors of the front: each parastichy intersects the front at the tip of exactly one green vector. And likewise there are as many (five here) green parastichies as there are red front vectors.

instead increase almost simultaneously, keeping close to one another, yielding parastichy numbers of the form (n, n) or (n, n+1), for instance. Whorled patterns are but the most regular type of this much wider class of phyllotaxis where, in general, primordia do not appear simultaneously.

Developmental dynamics behind phyllotactic patterns

In order to validate the framework in which we will highlight the conditions leading to distinct phyllotactic patterns, it is useful to look first at the developmental dynamics that lead to their emergence. Phyllotactic patterns in plants are established at a microscopic level through the organogenic activity of the shoot apical meristem (SAM) and can often be traced back as far as the initiation of the cotyledons in the embryo. Microscopic observations indicate that leaf and flower primordia are initiated only in the peripheral region of the meristem [16,17]. From their site of initiation, the primordia are slowly advected away from the meristem, eventually turning into the different lateral organs of the plant (Fig. 1).

The first clear insight into the positioning of primordia in the peripheral zone came from the work of Wilhem Hofmeister who stated [18: p. 482–483] (translation by the authors):

> It is a striking experimental observation that new leaves (or axillary buds) emerge at those locations on the periphery of the sensitive area surrounding the growing tip of the stem (or stem girdle), which are farthest from the lateral edges of the existing leaves.

Although Hofmeister's statement is far from a mechanistic explanation of phyllotaxis, it conveys the essential idea that the position of new primordia is determined by the position of pre-existing primordia as though their presence at the periphery of the meristem inhibited the formation of primordium in their close vicinity. In the decades that followed, various types of ablation experiments have confirmed the inhibitory effect that older primordia have on the initiation of new primordia [16,19].

A mechanistic explanation for Hofmeister's rule has only appeared in the last two decades, which has opened many avenues of research [13–15,20]. The main actors are the plant hormone auxin and the auxin efflux transporter PIN, both of which interact in a process called polarized auxin transport (Fig. 2). PIN proteins help auxin move across cell membranes. But PIN proteins are also "polarized" by auxin: as a primordium initiates, they concentrate on the side of the cell adjacent to surrounding cells that have high auxin concentration. In other words, these two molecules are in a feedback loop where PIN proteins control the directionality of auxin fluxes, and auxin

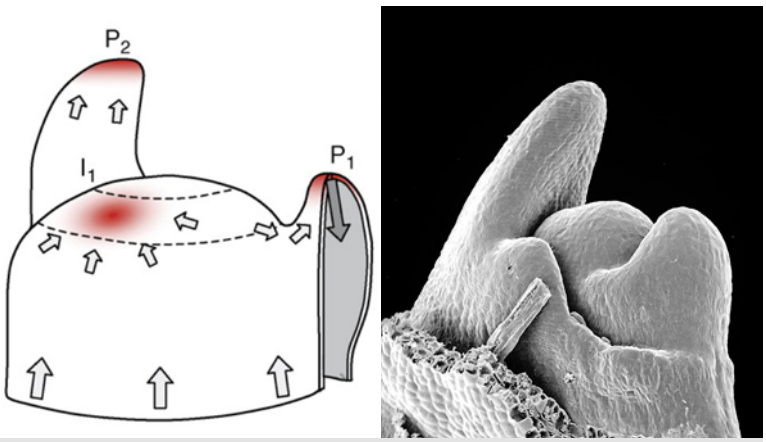

Fig. 2 Polar auxin transport. Left (courtesy C. Kuhlemeier): red shading indicates areas of high auxin concentration. Arrows show the direction that PIN proteins direct auxin to. PIN protein direct auxin to areas of greater concentrations, initiating primordia formation (I1). Nearby cells are depleted of auxin, inhibiting the initiation of other primordia near the new one. As the primordium grows, PIN starts directing auxin downward (P2 and P1) through the provasculature. Right (courtesy R. Rutishauser): electron micrograph of a *Muehlenbeckia* apex.

in turn controls PIN proteins localization. As a result, auxin flows where there is more auxin ("up-gradient flux"). In other words, PIN amplifies disparities in auxin concentration, making the uniform distribution of auxin an unstable equilibrium. Moreover, as an area around the meristem sees a surge in auxin concentration, marking the initiation of a primordium, its surrounding cells are depleted of auxin, and therefore no primordium can form close to a new one (at least not until enough auxin flows from the meristem to that zone in the periphery). This kind of coupled short-range activation and long-range inhibition, where the uniform distribution of some morphogen is an unstable equilibrium is a classical recipe for pattern formation, reminiscent of the instability Alan Turing promoted as a mechanism for morphogenesis in general, but also specifically for phyllotaxis [21].

The essential interactions between auxin and the PIN protein are captured in some of the oldest models of phyllotaxis. Schwendener [2], in particular, formulated a model of phyllotaxis that involves incremental stacking of disks (or similar shapes) on a cylinder, each disk representing the inhibitory footprint of a primordium sitting on the meristem. As we will show below, this process can reproduce all the patterns recognized in phyllotaxis, including the famed Fibonacci patterns and the newly discovered quasi-symmetric patterns.

To analyze the phyllotactic patterns and their transitions, we make use of the concept of primordia fronts, which can be seen as the latest layer of primordia formed in the peripheral zone of the meristem [6,22]. These fronts can be represented by the zigzagging lines joining the centers of disk-shaped primordia (Fig. 1). We call the numbers of zigs and zags in a front, the front parastichy numbers. When the pattern is regular enough, as in the pineapple above, they correspond to the usual parastichy numbers. But front parastichy numbers continue to exist even during transitions, and provide a way to understand them. For this reason, and others that we explore below, fronts are central to our study of transitions.

Before describing in greater detail our model and the results we obtained, we exploit the concept of fronts to give a brief explanation of why Fibonacci patterns and quasi-symmetric patterns are common in plants.

Why Fibonacci?

Fig. 3 presents the analysis of a (5, 3) → (5, 8) transition which encapsulates our answer to this classical question.

Fig. 3 and its caption raises some questions:

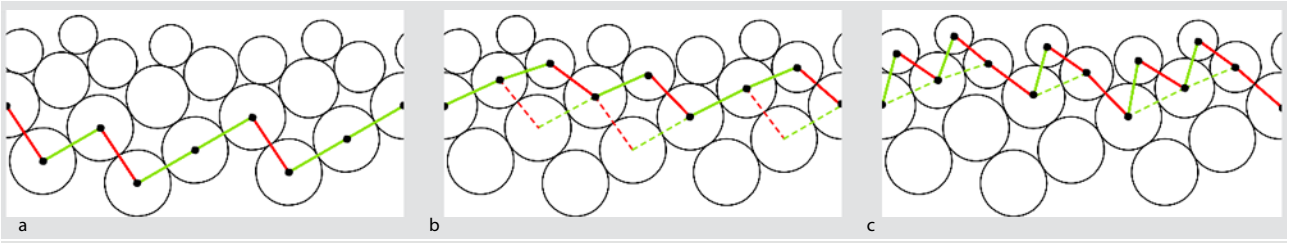

Fig. 3 Fronts as Fibonacci machines. In **a**, the front has parastichy numbers (5 , 3): five green up-vectors, three red down-vectors. This does not change in the front shown in **b**, as the transitions between the two fronts are all "quadrilateral", where a pair of down- and up-vectors is exchanged for a pair of up- and down-vectors. But, since the disks are smaller, the vectors are all getting more horizontal. Moreover, since there are five green vectors to cover the same vertical distance as the three red vectors, the green vectors are more horizontal than the red ones. The transitions above that front (**c**) cannot be quadrilateral as the angles in adjacent pairs of down- and up-vectors (notches) are too wide. They must be triangle transitions and, for the new disks to be in the lowest possible positions, the triangles have to rest on the most horizontal vectors. These are the green vectors here. Hence, each green vector gives rise to a (rotated) green vector and a new red one. The number of green vectors does not change, but the number of red vectors is increased by 5. The fronts have geometrically produced a Fibonacci step: (5, 3) → (5, 3+5) = (5, 8).

- How did we get to a (5, 3)-front in the first place? This figure shows only one step of a recursive process. Plants often start with a (1, 1)-front, or a (2, 2)-front which transitions to (2, 3) or (3, 2). The transitions (1, 1) → (2, 1) → (2, 3) → (5, 3) would follow the same basic mechanism as seen in this figure (see Fig. 11 for a complete simulation.)
- How prevalent is this Fibonacci transition scenario in phyllotactic patterns? The model chosen, and the concept of fronts make an answer possible to this question: if the early fronts are regular enough and the diameter of the disks decrease slowly enough, the pattern will undergo only Fibonacci transitions (at least for a while). But the scenario outlined in Fig. 3 can be systematically detected over a large parameter space, and found to be occurring on patterns far away from regular lattices (Fig. 15). See section "Heuristic arguments for MGRS and QSS" for a heuristic argument for its prevalence. Part II [23] of this work will provide clear botanical examples of such Fibonacci transitions, both increasing and decreasing.
- How does this argument compare to previous ones in the literature? The drawing of transitions such as Fig. 3 is not new: Schwendener [2] and van Iterson [3] drew very similar pictures more than a hundred years ago. To our knowledge, however, the simple explanatory scenario, outlined in Fig. 3 that fronts, together with their parastichy numbers and regularity provide is new. van Iterson [3] made an argument that is the most comparable to ours. He defined "zigzaglinie", which are also fronts, but with the restriction that the up- and down-vectors meet at right angles. He then elaborated a Fibonacci transition scenario, using the zigzaglinie only away from transitions, claiming that transitions necessarily passed from a zigzaglinie that is part of a Fibonacci lattice to one of higher order. In his argument, he assumes that the disk-stacking process naturally converges to these square fronts. While our simulations are a witness that these claims cannot be true, his arguments are still very rich in ideas, and should not be dismissed. Another analysis of Fibonacci transitions is provided by Mitchison [24], in the context of stacking of disks of constant radius on a widening cone (a convention also adopted in [4]). The rather rigorous argument that Mitchison provides is unfortunately only valid for slow transitions of patterns that are close to lattices, and, crucially for his argument, have the same ordering as lattices. We believe that the argument based on fronts is not only simpler, but it applies to much more general and irregular patterns and enables one to explore the fuller extent of the Fibonacci phenomenon and the boundaries of its validity.

Why quasi-symmetric?

When the conditions for Fibonacci transitions are violated, i.e., when an initial front is too irregular and/or the disks shrink too quickly, we observe, in our simulations, a predominance of quasi-symmetric patterns: those whose parastichy numbers are

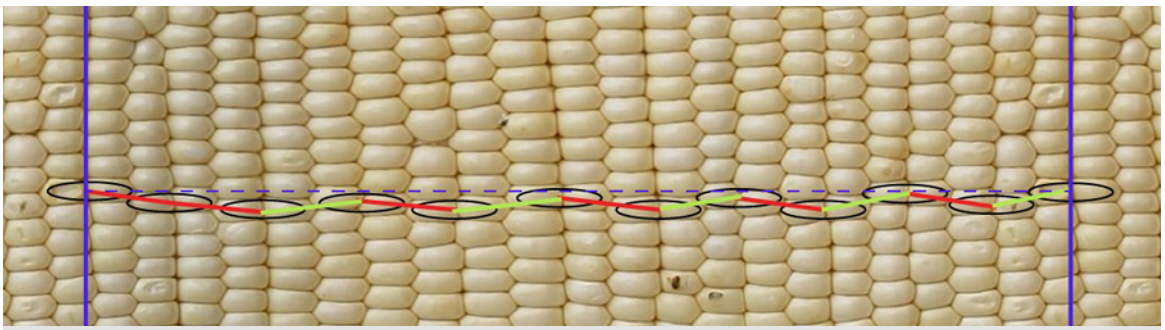

Fig. 4 Quasi-symmetric corn. A detail of an unrolled corn cob, of phyllotaxis (5, 6). The two vertical purple lines show the period of the cylindrical pattern. Each primordium gives rise to a pair of adjacent kernels, as indicated on the front.

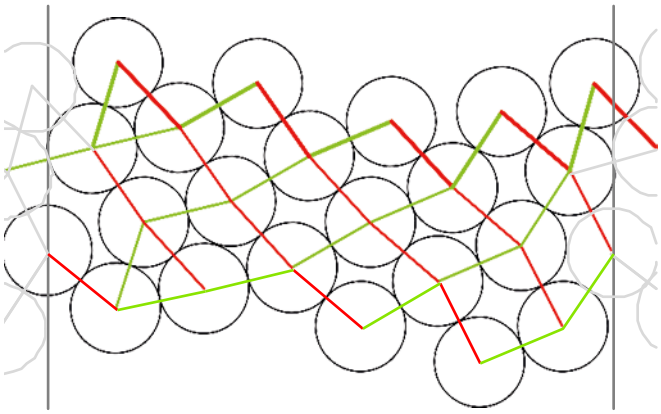

Fig. 5 Drift toward symmetry. An irregular (5, 3)-front yields a (5, 5)-front, via a combination of three triangle and one pentagon transitions.

equal or are almost equal. We believe that this kind of pattern is relatively frequent in nature (Fig. 4), although it is usually not mentioned in the literature, or is taken as a result of extreme condition/selection, as is the case of maize.

Again looking at the geometry of the more irregular fronts (see Fig. 5) and/or of transitions of patterns with rapidly shrinking disks, we are able to detect a large set of these patterns numerically (section "Sweep through the set of (1, 1)-fronts with varying radius decrease rate"). We also give heuristic arguments (section "Heuristic arguments for MGRS and QSS") for their occurrence. In particular, we reveal some of the mechanisms at play that lead to a drift toward quasi-symmetry of patterns with initial fronts of parastichy numbers distant from one another. An instance of this mechanism is shown in Fig. 5. Part II [23] provides more botanical examples of these patterns and evidence of the route to quasi-symmetry as explained with the model here.

Structure of the paper

We made the choice of keeping away from mathematical technicalities in this paper, preferring to highlight the simplicity of the concepts and arguments, and systematic simulations. We first define rhombic tilings, fronts and all the average measures they give rise to (front parastichy numbers, average divergence, resultant, irregularity, see section "Disk-stacking model and front transitions"). We use these new measures to analyze two representative patterns, one Fibonacci, the other quasi-symmetric (section "Simulating and measuring pattern formation"). We show that they present characteristic asymptotic patterns: their ratio of parastichy numbers tending to the golden ratio for Fibonacci like transitions, and to 1 for quasi-symmetric transitions. We use these to formalize two scenarios yielding Fibonacci-like and quasi-symmetric patterns, and perform large numerical studies of simulations, sweeping over parameter spaces for patterns starting with (1, 1)-fronts (monocot type; section "The Fibonacci and the quasi-symmetric transitions scenarios") and (2, 2) (dicot type; Appendix S2). These studies show the prevalence of Fibonacci phyllotaxis in conditions of sufficient regularity and lowrates of diameter decrease. In much of the rest of the parameter space, we detect a tendency toward quasi-symmetric patterns. We then give some heuristic arguments for why Fibonacci and quasi-symmetric patterns occur when they do (section "Heuristic arguments for MGRS and QSS"), providing some mathematical framework along the way. Finally, we conclude with reflexions on the broader meaning of these findings (see "Conclusion").

Disk-stacking model and front transitions

In this section, we describe the classical disk-stacking model. We then introduce the concepts of primordia fronts and their characteristics (parastichy numbers, resultant and average divergence), central to our geometric analysis of phyllotactic transitions.

Disk-stacking

Schwendener [2] introduced several geometric models of stem and primordia shapes. It turns out that using the more botanically looking shapes he introduced does not seem to add much to the understanding of the geometric mechanisms of phyllotactic transitions [24,25]. We choose to concentrate on his simplest choice of shapes: the cylinder for the stem, and disks for the footprint of the primordia on the stem. This choice simplifies both computer simulations and the geometric analysis, and seems to capture the main mechanisms of phyllotactic transitions.

Expanding on Hofmeister's observations, Schwendener observed that, as primordia first form, they are in close contact, with no overlap, and are of comparable size [26]. In light of this, Hofmeister's[1] rule can be modeled as **disk-stacking rule**: *new disks are incrementally added on the surface of the cylinder in the lowest available location above the existing disks, without overlapping them*.

The iterative disk-stacking process based on the repeated application of the above rule, would be entirely deterministic if it were not for the (rare) situations when there are two (or more) allowable places at the same lowest height. When this is the case, the order of placement of a disk in those lowest places usually does not matter, as different choices yield the same pattern after a few iterations. But at crucial times, placing a disk in one of the allowable lowest places precludes the placement of another disk in another nearby allowable lowest place, and the different choices do yield different configurations (for examples see [1] or [28]). Mathematically, the map defining the process is multivalued at these points. This case happens prominently when reducing the relative primordia size starting from an opposite leaf phyllotaxis (1, 1), the first primordium deviating from the opposite position has the choice between two symmetric possibilities. The choice will determine the chirality of the rest of the pattern [29], see section "Observation of a simulated fibonacci pattern formation".

Parameters variations

With this caveat, the disk-stacking iterative process is determined by two factors: the initial configuration of disks and the diameter b of the successive disks relative to the circumference of the cylinder. For simplicity, we will always assume that the cylinder has circumference 1. With this convention, b is just the diameter of the primordia. Variations of b are responsible for the phyllotactic transitions. To change continuously the parameter, we will assume that its value is given as a function $b(h)$ of the height h of the center of the disk. In this paper, we simply assume the relation between b and h to be linear. The relation between b and the disk number, which one can think of as time, may be much more complicated.

Botanically, the size of a primordia is rather universal and constant, around 50 µm, and the phyllotactic transitions happen when the radius of the meristematic zone (or radius of the cylinder) changes, such as schematized in [4] or [24]. We assume here that it is the relative primordia diameter which is important, and that possible quantitative difference between the two approaches have a minimal impact. Such minimal impact of geometry was also found by van Iterson [3] or [25]. In other words, we assume that for their dynamical properties both approaches are qualitatively the same.

[1] There is no trace in Hofmeister's work of a regularity in primordia size, or time, as was later attributed to him. Schwendener was the first to add primordia size regularity [26]. This principle was overlooked until R. and M. Snow restated it based on their botanical experiments and stressed its importance [27].

Fronts and their parastichy numbers

Fronts. Informally, a front is the ring formed by the most recent primordia around the apical meristem at a given instant of the growth [22]. It includes all the necessary information for the positioning of the next primordium, and not more. To determine all the successive fronts from an already formed pattern (either botanical or produced by a model), we need to understand their geometrical properties. We use the disk-stacking process to guide us.

Fig. 6a shows the evolution of the disk-stacking process from a rather irregular scattering of disks (in gray). Because each new disk is tangent to two below, they soon organize into zigzagging rings of tangent disks encircling the cylinder[2]. Similarly, given a "grown" pattern, we can draw zigzagging rings of disks of the pattern encircling the cylinder. To figure out which of these rings are fronts, we translate in geometrical terms the rule that a front should contain the necessary and sufficient information for future growth (i.e., future iterations) at a given time.

Consider a few examples. The ring {10, 7, 4, 6, 9, 11, 8, 10} has more than the sufficient information needed to determine the disk accretion after Disk 11: all the necessary information is contained in the ring {10, 7, 9, 11, 8, 10} as the Disks 4 and 6 have no direct bearing on the rest of the pattern. The ring {10, 7, 4, 6, 8, 10} does not represent all the sufficient information about the pattern up to Disk 10, as it omits Disk 9, which does have a bearing on the future of the pattern. The lowest ring {5, 2, 4, 1, 3, 5} does not have either of these shortcomings. It does not fold over itself as our first example did; and the disks above it are higher than the disks of the ring, contrary to our second example.

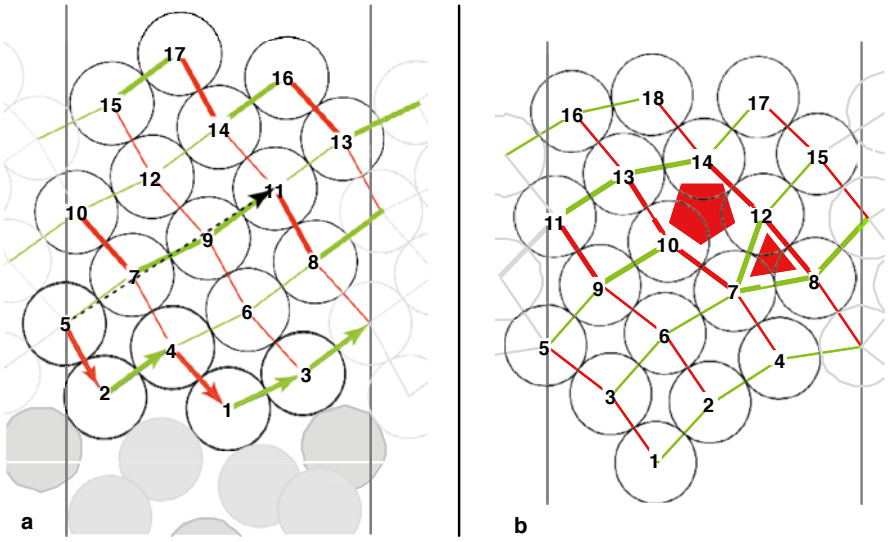

Fig. 6 The disk accretion model. The figures represent portions of unrolled cylinders where, in each, the left and right edges are identified. Disks of constant radius are stacked one at a time, on top of existing disks, without overlap and in the lowest place possible. **a** The semi-random initial configuration of gray disks gives rise to a pattern with recognizable parastichies (three red and two green). By convention, we represent right-handed parastichies in green and left-handed in red. This is a rhombic tiling: all transitions are quadrilateral. The three rings of tangent disks joined by bold red and green vectors are examples of fronts for the pattern, of label 5, 11, and 17, respectively. Reading from left to right, the left-handed red parastichies gives red vectors pointing downward, while the right-handed parastichies gives green vectors pointing upward. Fronts in this configuration all have parastichy numbers (3, 2), defined by the numbers of up- (green) and down- (red) vectors in each front. This is a Period 6 pattern: the three fronts in bold are translates from one another, by the dashed vector joining point n to point n+6, which is the resultant of the fronts in this pattern. **b** A pattern with varying front parastichy numbers, starting as a (3, 2), transitioning to (3, 3) via a triangle transition at 12, and back to (3, 2) with the pentagon transition at 14. The transitions are marked by a solid triangle and a solid pentagon, colored red to signify the type of vectors whose number is changed by the transition. This creates a triangle–pentagon pair.

[2] Given reasonable conditions, one can show this always happens (Golé and Douady, unpublished manuscript "Convergence in a disk-stacking model on the cylinder").

This brings us to the following definition, which is applicable to data analysis as well as to our model (see [6] for a more formal one): *a front is a zigzagging ring of primordia encircling the cylinder, each primordium being tangent to one on its left and one on its right. Moreover, any primordium above the front must be higher than any primordium of the front.*

In the disk-stacking process, we label a front by its highest disk index. For instance, the front {5, 2, 4, 1, 3, 5} is the front at 5. A front can also be described by the front vectors which join the center of each primordium to its tangent neighbor on the right, as we have represented on the front at 5. The front vectors split into two categories: up and down according to whether their slope is positive or negative[3]. Throughout this paper, we color up-vectors in green and down-vectors in red.

Given a pattern of primordia, each tangent to a primordium on the left and one on the right, one can follow a simple algorithm to find the front at a given primordium *P*: starting at *P*, go to its right tangent neighbor below. From then on, continue to the right, picking at each step the highest tangent neighbor available without ever going higher than *P*. The process must bring you back to *P*, where the front ends.

Front parastichy numbers. The pattern arising from the simulation shown in Fig. 6a has parastichy numbers (3, 2): three red (left-handed) parastichies and two green (right-handed)[4]. These numbers can be conveniently read off from any front in this configuration, by simply counting the three (green) up-vectors, and the two (red) down-vectors of the front. This one-to-one correspondence, the number of up- (green) vectors giving the number of down- (red) parastichies and vice versa, simply arises from the fact that each red parastichy lands at the tip of exactly one green vector in the front, and each green parastichy lands at the tip of exactly one red vector in the front. We call the pair of numbers of up and down-vectors (in that order) of a front the front parastichy numbers.

Front parastichy numbers capture the state of a pattern at any given time. In Fig. 6b, for instance, the configuration starts with (3, 2)-front at 5, and the parastichy numbers remains (3, 2) until the front at 12 where there is a *triangle transition*, where the parents (Disks 7 and 8) of Disk 12 are adjacent. Two front vectors, the up-vector 7 → 12 and down-vector 12 → 8 replace the single up-vector 7 → 8, with a net addition of 1 to the down-parastichy number. As a result, the front at 12 has parastichy numbers (3, 3). Decrease in parastichy numbers occur when there is a *pentagon transition*. This is the case between fronts at 13 and 14 in Fig. 6b, where the two down-vectors 13 → 10, 10 → 7, and the up-vector 7 → 12 are replaced by an up-vector 13 → 14 and just one down-vector 14 → 12, lowering the up-parastichy number by 1. Transitions with *n*-gons for arbitrary *n* also occur but much more rarely. As a general rule, an *n*-gon transition incurs a reduction of the sum of the parastichy numbers by $n-4$[5].

Although Fibonacci transitions are most often described as a global change from one pair of parastichies numbers to another one, front parastichy numbers allow to view these transitions step-by-step. This is reminiscent of the local view of transitions adopted by Zagórska-Marek, involving phyllotactic triangular units [30].

Front dynamics

Triangular and pentagonal geometry of the transitions. The simple geometry yielding triangle transitions holds the key to the mechanism of Fibonacci phyllotaxis. These transitions occur in *notches* of fronts, where an up-vector follows a down-vector (see Fig. 7). The geometry of the notch is given by the *bearing angles* α, β that its vectors are making with the horizontal (α < 0 in the figure as the vector 10 → 7 is down).

[3] We use the convention that a horizontal vector is up.

[4] That these are Fibonacci numbers is not a coincidence, but derives from the choice of disk size and initial configuration.

[5] In crystallography, these local transitions, which change the number of alignment lines, are called dislocations. A triangle transition would be called a "+1" dislocation (adding one line) and a pentagonal transition a "−1" dislocation. As in our model, higher degree of dislocations such as a $-n$, $n > 1$, are possible, but very rare.

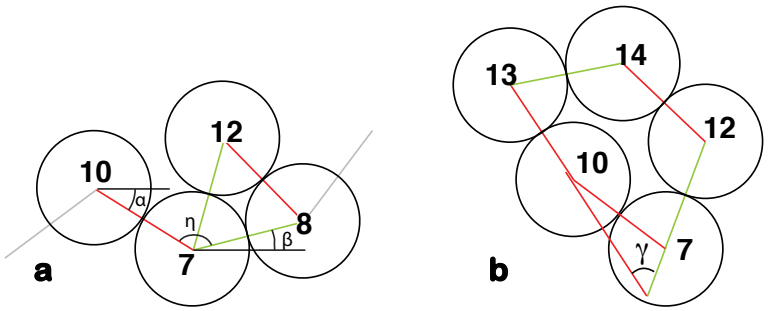

Fig. 7 Geometry of triangle and pentagon transition. **a** A triangle extracted from Fig. 6b. The notch angle η > 120° and the triangle occurs on the vector of smallest bearing angle: β < |α|. **b** Pentagon extracted from Fig. 6b. The angle γ < 60°.

Assuming for now constant relative diameter b of the disks, the condition for there to be a triangle is that the notch angle η satisfies η > 120° (note that η = 180° − β + α). If it were not the case, Disk 12 would intersect with either 10 or 8. This being given, a triangle transition could occur on either of the notch vectors. But to be on the lowest possible spot, it must occur on the vector which is the most horizontal. That is, in the case illustrated, the triangle occurs on the vector 7 → 8 because its bearing angle β is smaller, in absolute value, than α.

When the relative diameter *b* of the disks is a decreasing function of their height (as it will be in next section), the threshold angle η at which a triangle transition may occur is less than 120°. Indeed, in the example shown, were *b* to decrease with height, the effective angle of the notch would widen as the Disks 10 and 8 would be smaller than Disk 7. Moreover Disk 12 would be smaller as well. These all would contribute to a triangle transition potentially occurring for some η < 120°. And the faster the disks decrease with height, the smaller the threshold in η for a triangle transition to occur.

Pentagon transitions follow, in some sense, a reverse geometric rule to that of triangle ones. In this case, three vectors have to be considered in the notch. In the example of Fig. 7b, one condition is that the angle γ between the vectors 10 → 13 and 7 → 12 be less than 60°. Increasing *b* induces cascades of pentagon transitions, usually affecting the parastichy number corresponding to the most numerous front vectors, as they are the most likely to contribute to the side of the notch with two vectors. See [23] for botanical examples.

Regularization by pairs of pentagon/triangle transitions. Note that, in Fig. 6b, the triangle and pentagon transitions occur as an adjacent pair. This is a frequent situation in simulations with constant disk radius. At a triangle transitions, the new vectors are obtained from the base one by rotations of plus or minus 60° (Fig. 7a). However, the two vector angles after a pentagon are not so simple and involve a trigonometric solution of an equation involving three other vectors (Fig. 7b). Thus after a pair, one does not come back to the original front vectors. Even if the pairs happen periodically, and the parastichy numbers are periodical, which often happens when the fronts are not too disturbed, the pattern itself is not. One can show that such transition pairs have a regularization effect on the pattern. In this instance, the down-vectors 13 → 10 and 10 → 7 are transformed into the more aligned vectors 14 → 12 and 12 → 8. In general, these pairs may not be adjacent, but separated by some rhombi, appearing shifted along the corresponding parastichy (red in Fig. 7b).

Rhombic tilings. In Fig. 6a, the pattern shows only quadrilateral transitions. We call these patterns *rhombic tilings* [6]. If we view the disk-stacking process as a dynamical system (in a suitable space of configuration shapes), rhombic tilings are periodic orbits, of period equal to the product of its parastichy numbers. This makes intuitive sense: with quadrilateral transitions, the process of disk-stacking conserves the front's vectors, only changing their order by successively permuting adjacent up- and down-vectors at each iteration. With a finite size cylinder, and finite number of vectors, after each pair of up- and down-vectors has been permuted, the original order of

these vectors and thus the geometry of the front returns to its original state. Thus in a rhombic tiling of parastichy numbers (m, n), the period is nm, the number of possible pairs of up- and down-vectors.

Rhombic lattices and the van Iterson diagram. The lattices chosen as geometric models of phyllotaxis since the Bravais brothers' work in 1837 [31][6], see also Fig. 9, are but one special kind of rhombic tiling: perfectly regular ones with equal up-vectors, and equal down-vectors. The rhombic lattices that arise from the stacking process are fixed points for the underlying dynamical system [6]: adding a disk does not change the shape of the front. In this sense the period of a lattice resulting from the disk stacking process is 1. Although a rhombic tiling can look close to a rhombic lattice, the variation of vectors in a tiling is an essential difference. Since the vectors are different in a rhombic tiling, adding one rhombus, and thus switching the order of two vectors of the front, changes the shape of the front. In general, this shape can only be restored after mn iterations[6].

Lattices were emphasized in most previous modeling and simulations. For instance in [25,29,33] either the simulation was let run for a very long time to ensure the convergence toward the perfect state or the irregular simulations were averaged, and the averaged reinjected as initial condition to hasten the convergence. Similarly, all the theoretical work, as in [3,5,34,35] only considered transitions between lattices, without considering the place of transition itself. Even in [24], where the presence of irregularities was recognized, the explanation of Fibonacci pattern transitions was done using lattices.

Each rhombic lattice is uniquely given by its generating vector between a point of the lattice and the next one up (Fig. 9). The set of all possible rhombic lattices can be represented by the van Iterson diagram which traces the generators of these lattices in the plane. It can be interactively visualized [36]; see also [5,34].

In [6] and Part II of this work [23], evidence is presented that rhombic tilings are actually a better model of constant parastichy phyllotaxis than the more restrictive lattices, as they fit plant data better, accounting for instance for permutations of order in the pattern observed by botanists [37]. Nonetheless, the set of rhombic lattices and its van Iterson diagram forms some kind of skeleton, and serves as reference for the much more complicated set of rhombic tilings.

Other typical patterns. The other kind of pattern encountered in simulations with constant radius are those presenting sequences of pairs of triangle and pentagon transitions, as in Fig. 6b. Interestingly, one can show – at least in simple cases – that these must converge to rhombic tilings: the pentagons slim down until they become a quadrilateral transition. Moreover, they can do so either in finite timewhere, after a final triangle–pentagon pair the pattern becomes a rhombic tiling, or infinite time, converging exponentially toward a rhombic tiling (Golé and Douady, unpublished manuscript "Convergence in a disk-stacking model on the cylinder").

Experimentally, patterns generated by the disk accretion process with disks of constant radius are limited to these two kinds, with very occasional hexagon transitions, or even rarer n-gon transitions.

To summarize, the disc-stacking model produces patterns containing possibly not only rhombi but also triangles and pentagons. Because of them, even at a constant parameter b, the pattern may still evolve and fail to be periodic. When there is no triangle nor pentagons, the disk-stacking becomes a periodic rhombic tiling, with a large period. A limit case of rhombic tilings is when all its rhombi are identical, yielding a rhombic lattice, with minimal period of 1.

Global front characteristics

Resultant vector. As we have said earlier, a front contains all the information of the pattern at a given time. In particular the front shows explicitly the possible

[6] It is interesting to note that this work was published 13 years before A. Bravais used lattices in his seminal study of crystals [32].

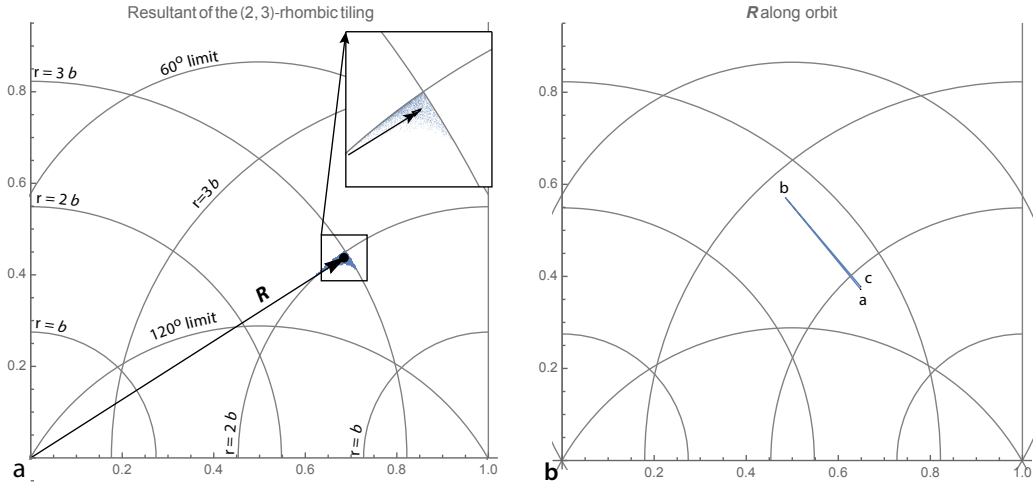

Fig. 8 Resultant vectors and their dynamics. **a** The resultant vector ***R*** of the rhombic tiling front from Fig. 6a is represented in the space of resultants of all possible fronts, between the 120° and the 60° limiting circles (gray, dashed). Because of the regularity of the fronts, the resultant is close to that of the lattice of same diameter (b) and parastichy numbers, located at the intersection of the circle of radius $3b$ centered at (0, 0) and the circle of radius $2b$ centered at (1, 0). The dagger-shaped cloud of blue points are resultants of thousands of randomly generated (2, 3)-rhombic tiling fronts with same b. Under the dynamics of the stacking process, the resultant of the rhombic tiling stays unchanged. **b** Resultants of the fronts in Fig. 6b . The figure represents the tips of the resultants of successive fronts in Fig. 6b, connected by lines. The original fronts of the pattern are more irregular than those of the rhombic tiling of Fig. 6a. Accordingly their resultant (Point a) is farther from the tip of the (2, 3) cell. After the triangle transition, ***R*** moves to the (3, 3) cell (Point b). It then comes back to a slightly more regular (2, 3)-front through the pentagon transition whose resultant (Point c) is closer to the tip of the cell.

irregularities of the pattern, when the up-vectors are not equals, and/or the down-vectors are not equal. However, this information can become too rich, especially when the parastichy numbers increase. One way of efficiently summarizing a pattern and the evolution of its fronts, while still keeping some information on its irregularity (which the parastichy numbers alone do not), is to look not at all the up-vectors of a front, but at their sum. We call this sum the resultant vector of a front. Since the sum of the up-vectors and the sum of the down-vectors must add up to the vector (1, 0), the vector $\boldsymbol{R}' = (1, 0) - \boldsymbol{R}$ represents the sum of the down-vectors of the same front. Given the diameter b of the disks in a front, we can retrieve the parastichy numbers from the lengths of $\boldsymbol{R}$ and of $\boldsymbol{R}'$. Specifically: $m = [||\boldsymbol{R}||/b]$ and $n = [||\boldsymbol{R}'||/b]$, where $[x]$ is the smallest integer greater than x.

The deviations from integer values of $||\boldsymbol{R}||/b$ and $||\boldsymbol{R}'||/b$ give an indication of the irregularity of the front. In a planar representation, we can thus analyze the resultant vector and its dynamics by drawing the grid of circles of integer multiples of b from (0, 0) and (1, 0). The cell the resultant falls in gives the parastichy numbers. The top of the cell is the resultant of the lattice of same disk diameter and parastichy numbers. The irregularity of the front can be visualized by how far from the top of the cell ***R*** is, as seen in Fig. 8. Because the front of a rhombic tiling has angle constraints between each pairs of its up- and down-vectors, its irregularity is accordingly constrained. The set of resultants of rhombic tilings of parastichy numbers (m, n) is thus rather limited, forming a dagger-shaped region at the top of the corresponding cell, see Fig. 8a inset.

The resultant vector, as it remains two-dimensional even when the number of front parastichy numbers varies, can be followed through the evolution of the front easily. Each transition (triangle then a pentagon in Fig. 6b), changes the parastichy numbers hence the vector position in the grid of circles, as shown in Fig. 8b. The resultant representation of the stacking process can be thought of as a 2D projection of the high dimensional phase space of its sub-tending dynamical system.

Average divergence angle. The resultant provides a way to compute an average divergence angle over a front. We essentially follow Bravais brothers' [31] (see also [5,34])

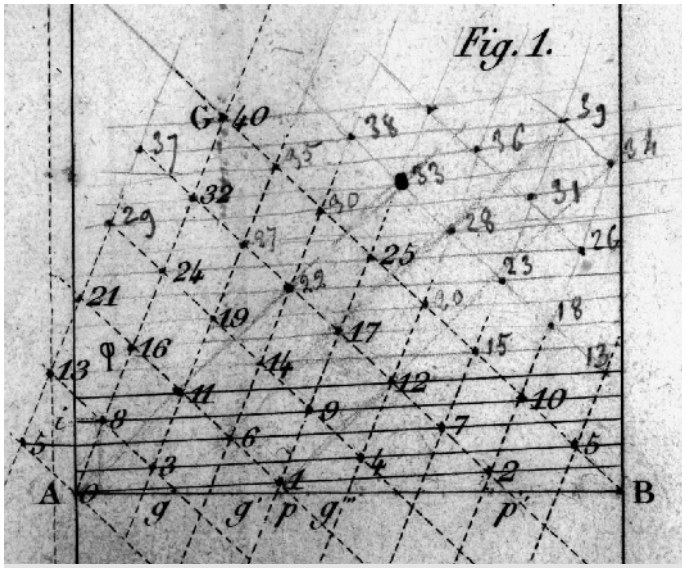

Fig. 9 Lattice and its parastichies. An original drawing of a (not rhombic!) cylindrical lattice of parastichy numbers $(m, n) = (5, 8)$ by the Bravais brothers [31]. The resultant joins Point 0 to Point 40 $= 5 \times 8 = mn$. The first point after 0 on the resultant is 8. To compute the x-coordinate of Point 8, the Bravais multiply the x-coordinate of Point 1 (the divergence angle x_1) by 8, and subtract the number of turns one makes on the generative helix (lower slope lines) to get there. So $x_8 = 8x_1 - 3$. Likewise, $x_5 = 5x_1 - 2$. The numbers $\Delta_8 = 3$ and $\Delta_5 = 2$ are called the encyclic numbers. Note the Bézout identity $8\Delta_5 - 5\Delta_8 = 1$.

pioneering work on lattices using their own figure in Fig. 9. In a cylindrical lattice of parastichy numbers (m, n) ((5, 8) in the figure), the resultant goes from base Point 0 of the lattice to Point mn (Point G in the Bravais' picture). The first of the m points it encounters on the way is Point n. That point has coordinates $x_n = nx_1 - \Delta_n$, $y_n = ny_1$ where Point 1 $= (x_1, y_1)$, and x_1 is the divergence angle (in unit of circumference) between successive primordia, y_1 is the vertical rise between successive primordia. The positive integers Δ_n, Δ_m are what the Bravais called the "encyclic numbers", the number of times the regular generative spiral wraps around the cylinder between the base Point 0 and points m and n, respectively. When m and n are coprime[7], Bravais showed that these numbers are linked by the relation:

$$n\Delta_m - m\Delta_n = 1, \left[\frac{\Delta_n}{n}, \frac{\Delta_m}{m}\right] \subset [0, 1] \qquad \textbf{Eq. 1}$$

This defines a unique pair $(\Delta m, \Delta n)$. This relation is well known in number theory as the Bézout identity.

The resultant $\boldsymbol{R} = (\boldsymbol{R}_x, \boldsymbol{R}_y)$ for this lattice thus satisfies $\boldsymbol{R}_y = y_{mn} = my_n = mny_1$ and $\boldsymbol{R}_x = x_{mn} = mx_n = mnx_1 - m\Delta_n$[8]. If we keep this last expression we can thus derive the divergence angle by:

$$x_1 = \frac{R_x}{mn} + \frac{\Delta_n}{n} \qquad \textbf{Eq. 2}$$

Although we derived this formula for a lattice (with identical up-vectors and identical down-vectors), we can extend its definition to any front. Thus, given a front of parastichy number (m, n), and $\boldsymbol{R} = (\boldsymbol{R}_x, \boldsymbol{R}_y)$ its resultant, we define the average divergence angle of the front as:

$$average\ divergence\ = \frac{R_x}{mn} + \frac{\Delta_n}{n} \qquad \textbf{Eq. 3}$$

The Bravais used this averaging formula to measure the divergence angle in plants. Finding the generative spiral on a stem can be challenging. Finding points m and n is much easier, as one follows the parastichies. But in the process, one looses track of the irregularity of the structure.

Front irregularity. To measure the irregularity of a front we take the largest deviation from their mean of the up-vectors, normalized by the length of the mean. We then do the same for the down-vectors, and take the product of these two values. For an illustration of this concept, see Fig. 10.

In fronts of constant diameter b, this notion is almost equivalent to measuring the area of the surface built by drawing segments between the resultant vector and each of the arcs of circles bounding above the cell it belongs to.

Closing words about front characteristics. Fronts, their parastichy numbers, resultant vectors and average divergence angles are ideal tools to numerically analyze a pattern and its transitions: it is quite easy to write programs that find successive fronts and compute their parastichy numbers, resultant vectors, irregularity as well

[7] When m, n are not coprime, we replace 1 by their greatest common divisor, $\gcd(m, n)$ in Eq. 1.

[8] Following van Iterson we can also compute this position along the other spirals, which is the nth point along it, up to a full turn of the cylinder, so $mnx_1 - m\Delta_n = x_{mn} = 1 - x_{nm} = 1 - nx_m = 1 - (mnx_1 - n\Delta_m)$. Equaling the first and last expressions gives the Bravais–Bézout relation. Erickson also used the properties of this mnth point

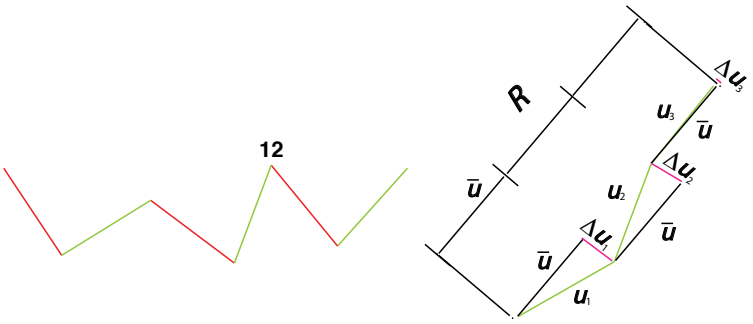

Fig. 10 Measure of a front's irregularity. On the left, the front at 12 from Fig. 6b. On the right, its up-vectors $\boldsymbol{u}_1$, $\boldsymbol{u}_2$, $\boldsymbol{u}_3$ put end to end, forming the resultant $\boldsymbol{R}$. The average up-vector $\overline{\boldsymbol{u}}$ is $\boldsymbol{R}/3$, and the vectors $\Delta\boldsymbol{u}_k = \boldsymbol{u}_k - \overline{\boldsymbol{u}}$ with k = 1, 2, 3 measure the deviation from the mean. The same can be done with the down-vectors. The maximum relative deviation from the mean up-vectors in this case is $||\Delta\boldsymbol{u}_1||/||\overline{\boldsymbol{u}}||$.

as their average divergence angles. It would be much harder to write one that detects and counts the classical parastichies, especially when there are transitions and their numbers vary. This and their ability to detect local transitions make fronts with their parastichy numbers, irregularity and resultant vectors central to this work.

Simulating and measuring pattern formation

As Schwendener and van Iterson had already observed [2,3], Fibonacci-like transitions often occur as the relative diameter b of the disks deposited decreases. The fronts point of view makes it clear why at least one of the parastichy numbers should increase as the disks decrease in size. Indeed, as the disks shrink, their number in a front, and the number of vectors connecting them must eventually increase in order for the front to reach around the cylinder. But our description of front transitions above shows that changes of their parastichy numbers happen through local events, either triangle or pentagon transitions, mostly. How, when, and why the local increase in parastichy numbers should globally follow the Fibonacci sequence is what this section and the next will seek to explain from the geometry of transitions. How, when, and why the local increase in parastichy numbers should not follow the Fibonacci sequence, and to what it then leads is what this section and the next will also seek to explain. Our underlying claim is that semi-local, front-averaged measurements of parastichy numbers, divergence angle, regularity, etc., are the appropriate tools for understanding phyllotactic pattern transitions.

Observation of a simulated Fibonacci pattern formation

Fibonacci transitions. The ideal case. Fig. 11a shows a typical simulation of the disk-stacking process starting from a (1, 1)-front, such as it would be encountered in a monocot embryo where a single large cotyledon is present. We have let the diameter of the disks decrease linearly with their height [specifically here: $b(h) = -0.1h + 0.34$]. Observe the Fibonacci progression of the front parastichy numbers: (1, 1) → (2, 1) → (2, 3) → (5, 3) → (5, 8) (in Fronts A, B, C, D, E, F).

Looking closer, we notice that the transition patterns are remarkably similar to those that Schwendener and van Iterson had painstakingly drawn by hand more than a century ago (compare Fig. 11a with Fig. 37 and 38 in [2] and Tab. XIII in [3]): the fronts go through relatively long phases of quadrilateral transitions, followed by clusters of triangle transitions (as highlighted by solid triangles in the figure). In the quadrilateral transition phases, note that the up-vectors of a given front are nearly parallel, and so are the down-vectors. Moreover this regularity is preserved after transitions.

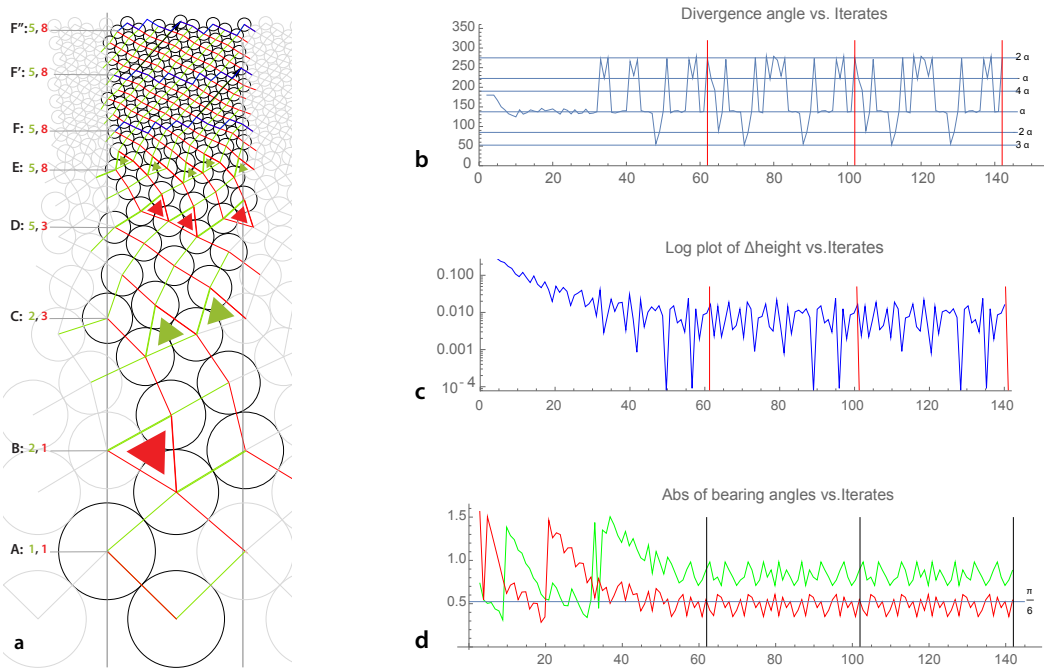

Fig. 11 Fibonacci transition in a simulation. **a** Disk-stacking simulation starting with a (1, 1)-front (A) of disks of equal diameter $b = 0.35$. The size of the subsequent disks is decreased linearly with height until it reaches $b = 0.048$, at iteration 49, after which it is kept constant. Four series of triangle transitions occur (marked by solid triangles), yielding fronts of Fibonacci parastichy numbers (2, 1), (2, 3), (5, 3), and finally (5, 8). The triangle transitions only occur on the most horizontal vectors, which correspond to the highest parastichy number. Thirteen iterations after 49, the pattern locks into a (5, 8)-rhombic tiling, of period 40. Three isometric fronts (F, F′, and F″) are underlined in blue, with the resultant vector (black) translating one into another. **b** Plot of the successive divergence angles (in degrees). After converging to a value approximately equal to the golden angle $\alpha \approx 137.51°$ in the first 30 iterations, the divergence angle starts oscillating between multiples of α, indicating switches in the order of successive disks. These fluctuations do not disappear, but become periodic of period 40 when the pattern becomes a rhombic tiling. Two periods are marked by vertical lines that correspond to the blue fronts in **a**. **c** Log plot of the height differences between the successive primordia. Whereas the differences decrease, the fluctuations remain large. Again, note the period 40 of these fluctuation in the rhombic tiling phase. **d** Graph of the (absolute value of) the bearing angles (in radians) that the newly created front vectors form with the horizontal (up: green, down: red), showing their global decrease and separation between transitions, and the switching of roles after transition.

As a result, when there are more up-vectors than down-vectors in a front, the down-vectors are steeper. In Front B for instance, there are two up-vectors and one down, and the down-vector is necessarily steeper: it decreases the height by the same amount that the two up-vectors increase it.

As the disks shrink during the quadrilateral phases, since the fronts have a constant number of disks, the front vectors must become increasingly horizontal so as to keep encircling the cylinder. The triangle transitions occur when the front is too flat and the notch angles are too wide to allow quadrilateral transitions. As noted in section "Fronts and their parastichy number", the triangles occur on the most horizontal of the front vectors in a notch. Front C is the first front of parastichy numbers (2, 1) to be flat enough to allow a triangular transition. It has two up-vectors and one steeper down-vector. The triangle transitions must then occur on the two up-vectors, with a net increase of the down-parastichy numbers by 2 and no change in the up-parastichy number. Thus the parastichy numbers transitions from (2, 1) to (2, 1+2) = (2, 3), a Fibonacci transition. The two up-vectors after this transition are now steeper, as they have to cover the same height difference as that covered by the three down-vectors, and they are approximately equal. This sets the stage for a transition at Front E, where the triangles occur on the three down-vectors this time, yielding a transition from (2, 3) to (2+3, 3) = (5, 3). Other transitions are similarly explained. This, in a nutshell, is the "ideal" geometric mechanism for the Fibonacci progression of parastichy numbers. We will see in section "Sweep through the set of (1, 1)-fronts with varying

radius decrease rate" that this mechanism (the "monotone golden ratio scenario") is indeed predominant in a large parameter set sweeping over initial configurations and speeds of radius decrease. We will also use this ideal mechanism as a benchmark to understand how it fails in more irregular patterns.

Divergence angles and height differences. The divergence angles graph (Fig. 11b) measures the angle, around the cylinder (i.e., the horizontal distance) between the centers of the new disk and of its immediate predecessor. One remarkable observation is that the divergence angle first converges to the golden angle [$\alpha = (3-\sqrt{5})/2 \approx 0.381966$ in unit of circumference or $\alpha \approx 137.508°$ in degrees] at least until Disk 28. That is, the divergence angle is not far from that of lattice fronts of the van Iterson diagram with corresponding b during this phase. After that it oscillates widely, but between multiples of the golden angle, a phenomenon observed in [38], Fig. 9 for a similar model. Since the Bravais brothers [31] made a connection between the golden angle and Fibonacci phyllotaxis, convergence to this angle has been the most common validating test for models of phyllotaxis since the 1980's. What happens after Disk 28 could disqualify our model, or at least this simulation: its divergence angle does not stay close to the golden angle for large parastichy numbers, even after the parameter b is kept constant. Yet the parastichy numbers are neat and steady, happily jumping from a Fibonacci pair to the next in a monotonic way (see Fig. 12b, and also [38] and Fig. 10). This shows the limitation of the criterion of convergence of the divergence angle to the golden angle as a Fibonacci phyllotaxis detector: for larger parastichy numbers, relatively small irregularities will result in disks switching their stacking

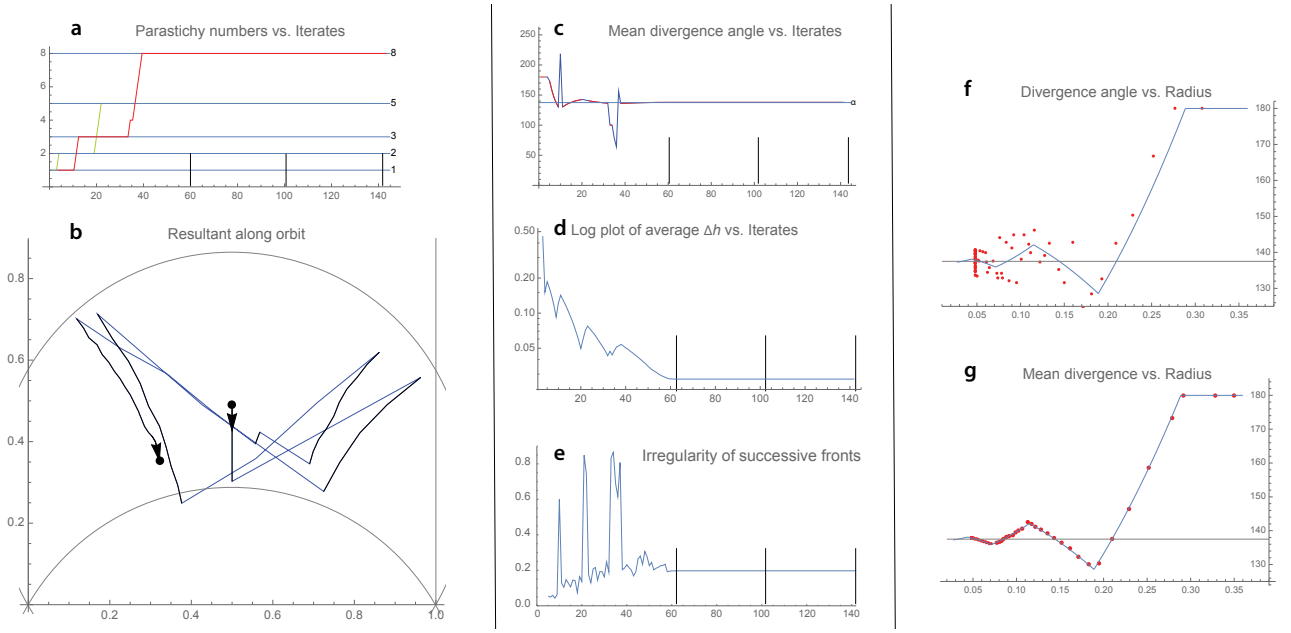

Fig. 12 Front statistics of the transition simulation. Analysis corresponding to the simulation shown in Fig. 11a. In **a**, **c**, **d**, **e**, we've indicated the two periods in the rhombic tiling phase. **a** The parastichy numbers of the successive fronts. Starting from (1, 1), one observes the successive increases of one side while the other one stays constant. The two periods of the rhombic tiling phase are marked by vertical dashed lines. **c** The tips of the successive resultant vectors $\boldsymbol{R}$ plotted in the rolled out cylinder. As the primordia diameter decreases, $\boldsymbol{R}$ moves down making an arc toward the mid line (black curves). At the transitions (in blue), either $\boldsymbol{R}$ increases in size (when the number of up-vectors increases) while the length of $\boldsymbol{R}'$ stays essentially constant, or the converse. This result in $\boldsymbol{R}$ moving up diagonally to the right or to the left respectively. **c** The mean divergence angle of the successive fronts as deduced from the resultant vector. During the transitions (in blue), the mean divergence ceases to make much sense since its computation relies on the number of parastichies, which is in a transiting state. The mean divergence becomes constant when rhombic tiling mode is reached **d** The mean height Δh's overall decrease over successive fronts. Note that Δh increases during triangle transitions, and stays constant during rhombic tiling phase. **e** The irregularity of the successive fronts shows sharp peaks at transitions, and otherwise a moderate increase from a small value. **f** The divergence angle plotted as function of the radius, together with the Fibonacci branch of the van Iterson diagram (in the radius/angle plane). The vertical accumulation on the left corresponds to the rhombic mode (when the radius is constant). The figure was truncated in the vertical axis, leaving out many outliers. **g** The mean divergence angle vs. radius shows a remarkable fit to the van Iterson diagram. The truncation only leaves out the transition points.

order – hence the wild oscillations between divergence angles close to multiples of the golden angles seen after Disk 28. A simple permutation in the order of appearance of two primordia lead to a "M" shape in the angles [33]. This switch can happen without great change in the overall geometry of the pattern. Reliance on the convergence of the divergence angle imposes a limitation on the speed of decrease of the radius and length of transition not often observed in plants. And indeed these types of oscillating patterns are seen in plants [1,23,27,39], and seem far from exceptional. The fluctuations in vertical spacing, also a sign of the order switching, are clearly visible in Fig. 11c. Instead of having a smooth decrease of order $1/n^2$, as one would expect from the prescribed linear decrease of diameters with height, the fact that primordia are in contact with previous ones of other diameters, and the irregularities, make their successive positions more and more irregular, even after b is kept constant.

Chirality. Note that, by symmetry, there are two allowable positions for the disk placed on Front A. The program placed one on the down-vectors (red) of the front, to the left. A disk placed on the up-vector would have been equally possible since it would have been at the same (minimum) height, but not both disks can be placed in the same configuration as they would overlap. The other choice of disk would have resulted in a mirror image of this pattern, with respect to the vertical. Hence the (2, 1)-Front B would be instead a (1, 2)-front, and more generally the parastichies would wind in opposite directions from those of this figure. Botanists relate this geometric choice to the chirality of the generative spiral (that connects successive primordia) of the plant, and it is widely believed that plants of a same species exhibit the two chiralities with the same frequency [40] – as reflected by the symmetry of the initial condition of our model. However, some observations show that it might not be the case, or more precisely that the initial conditions might not be symmetric themselves [41].

Front-based statistics

Fronts provide a variety of ways to measure the evolution of a pattern. They are the link between the local measurements of divergence, and height increment (Fig. 6), and the detection of the global notion of parastichies and their numbers. Whereas the Bravais brothers [31] had already presented a connection between divergence angles and parastichy numbers in 1837, their analysis (and that of van Iterson [3] and others) only works in the case of perfect lattices. Fronts give a handle on the geometry of patterns at a scale that can meaningfully make these connections, even during transitions, and thus far away from lattices.

Parastichy numbers graph. The transitions of the simulation shown in Fig. 11a can be monitored by the graph of parastichy numbers of fronts vs. the index of the highest point of the front (Fig. 12a). Because of our choice of initial condition (simulating early leaves in a monocot-like stem), both curves start at 1. The up- (green) parastichy number goes up by one at the third disk of the pattern, following the first triangle transition, yielding a (2, 1)-front. After that both parastichy numbers remain constant until Disk 9 (yielding the Front C): the transitions are all quadrilateral in that range. Accordingly, both parastichy numbers curves are horizontal between 3 and 9. Subsequent zones of triangle transitions yield the monotone increase of one of the curves, while the other remains constant. Zones of quadrilateral transitions yield parallel plateaus of the curves. All these features are easily detected by a computer program and form the base of our notion of monotone golden ratio scenario studied in the following sections.

Resultant graph. The resultant evolves in a characteristic "butterfly" manner along a pattern of Fibonacci transitions (Fig. 12a). During the quadrilateral phases, as the front vectors become increasingly horizontal, so does the resultant. Accordingly, the resultant traces curves (in black) going down toward the bottom circle, locus of resultants of rhombic lattices with notch angle of 120°. Before reaching this limit, at least one of the notch angles of a not perfectly regular front is greater than 120°. As the notch angles are large enough, triangle transitions occur and the resultant $\boldsymbol{R}$

goes up, as either itself, as sum of up-vectors or, in alternating fashion, its companion $\boldsymbol{R}' = (1, 0) - \boldsymbol{R}$ for the down-vectors, are augmented by new vectors. This creates a butterfly-like pattern which shows signs of convergence: the black curves are getting closer to one another, on the their respective sides. In the above example, this convergence process is cut short at iteration 62 when, because of the constant radius, all the fronts have the same resultant at about (0.32, 0.35). See Fig. 14 for a prolonged convergence of this pattern.

Mean divergence and height difference. Most of the local fluctuations seen in the divergence angle and height differences graphs of Fig. 11 are smoothed out in taking the front averages of these quantities (Fig. 12c,d). Since they average over an unchanging set of front vectors these averages are constant during the rhombic tiling phase. There are bumps in the height difference graph during transition, as subtle trace of the fact that the height increase in a triangle transition is greater than in a quadrilateral one. To understand this fact, visualize a quadrilateral transition on a three disks notch that is progressively opening up. The new disk is the child of the end disks. At a given point, the child of the end disks intersects with the middle disk, which is against the stacking rule. Instead, the new disk must be replaced, in a triangle transition, by a higher disk, child of an end disk and the middle one.

The average divergence angle displays jumps at transitions, which are artifacts of the definition of the encyclic numbers Δn, Δm. At the transitions, as the parastichy number is in a transiting state, the encyclic numbers are jumping, leading the average divergence angle points outside the window of Fig. 12e. But outside the transitions, the average divergence angle behaves almost exactly as if it corresponded to the divergence angle of the perfect lattice for that radius and those parastichy numbers. This is best seen in Fig. 12f. Average divergence angles of successive fronts are plotted as red points. The blue graph is a branch of the van Iterson diagram (in these coordinates). It traces the divergence angles of lattices of parastichy numbers following the Fibonacci sequence, as the radius of the disks decreases. Note the remarkable fit obtained by simply averaging the divergence angles of the entire front. Compare to the original data of individual divergence angles in Fig. 12e. This fit could be explained by the regularity of the fronts: the more regular a front is, the closer it is to a perfect lattice. Interestingly, the front can be close to a lattice globally, as evidenced by the great fit to the van Iterson diagram, and yet have its points' heights ordered differently, or even its sequence of up-/down-vectors in a different order as those of the lattice, permuting the stacking order of subsequent disks. Hence the great fluctuations in the divergence angle seen in Fig. 11b.

Observation of a quasi-symmetric pattern formation

Fig. 13a,b show a pattern exhibiting quasi-symmetry, where the parastichy numbers in this case remain at most two apart. To obtain this pattern, we started with a (1, 1)-front as before, and let the diameter b of the disks decrease rapidly with their height h [specifically here: $b(\mathrm{h}) = -0.27h + 0.388$]. This is almost three times faster than in the Fibonacci pattern of Fig. 11. One now observes a simultaneous and steady increase of nearly equal parastichy numbers. Note the pattern of almost simultaneous triangle transitions of alternating colors, in contrast with the previous Fibonacci transitions case where all possible triangle transitions of one color take place before the transitions of the other color start taking place. A striking fact is that the transitions in both directions are segregated in space. For instance one side (left) have up (red) transitions while the other (right) have opposite transitions, and they alternate. Moreover, many of these triangles happen so close to each other that they stack up in vertical pairs of opposite colors.

The parastichy numbers pull apart right after b stops decreasing (at Iteration 36), driven by spatially color-segregated pentagon and triangle transitions. From Fig. 13a, one can see that just after reaching the minimal diameter (at Iteration 37), there are still a lot of triangle transitions occurring. This shows that the resulting front has still a lot of wide notch angles due to the rapid diameter decrease, and enough irregularity for the notches to lean on one side or the other. At first the triangles appear

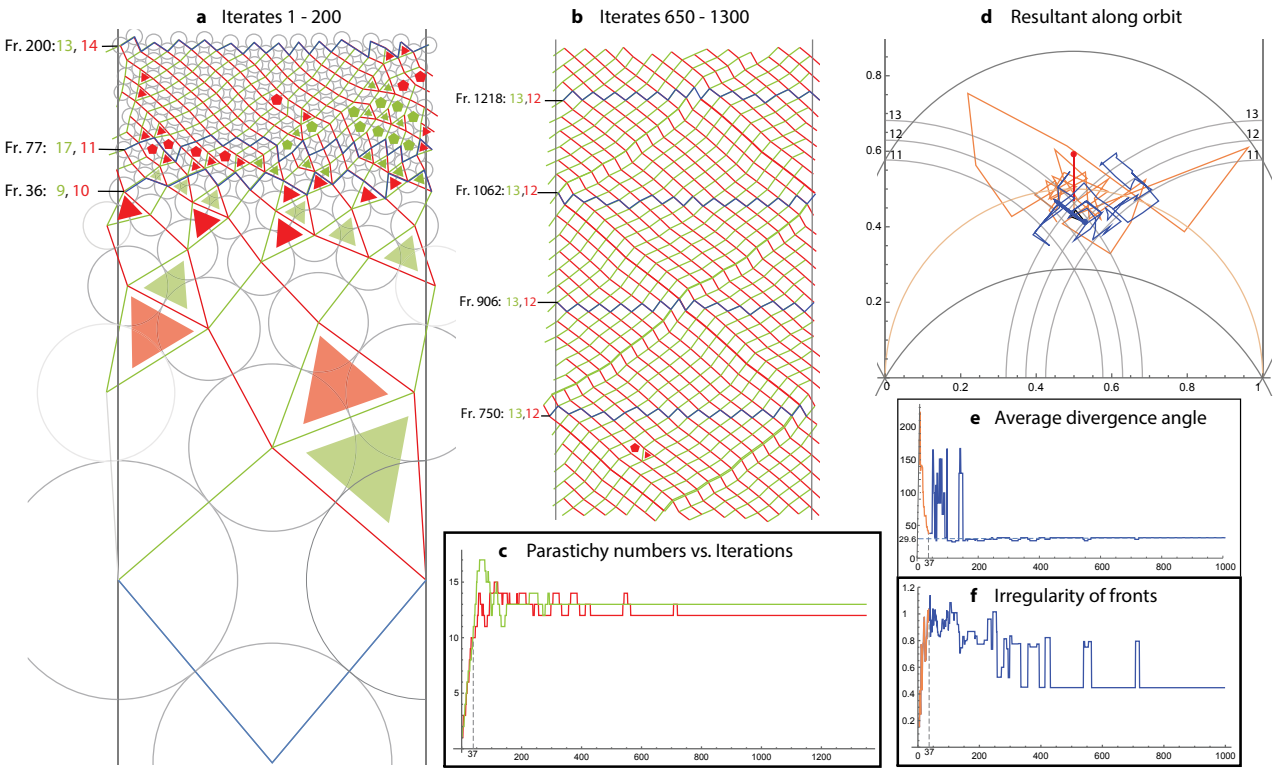

Fig. 13 Quasi symmetric transition. A quasi-symmetric pattern rising from a rapid decrease of the relative diameter *b*, until Iteration 36. The parameter *b* is then kept constant for the rest of the simulation. **a** Up to Front 36, the pattern undergoes triangle transitions in alternating directions, keeping the increasing parastichy numbers close together. After Front 36, as the radius is kept constant, a mix of pentagon and triangle transitions occur, in both directions. The parastichy numbers pull apart from (10, 9) to (11, 17), reaching maximum difference at Front 77. They then pull back together, converging to a quasi-symmetric (13, 12)-rhombic tiling after a long transition ending at Disk 721 with a last triangle–pentagon pair (**b,c**). **d** The tips of the successive resultant vectors, drawn on the unrolled cylinder, are joined by lines, colored orange for the first 36 iterations (phase of decreasing *b*) and then blue (constant *b* phase). Note the concentration of the resultants toward the center of the figure, where quasi-symmetry resides. **e** The average divergence angle converges towards a value just above 29.59°, which is the divergence angle of the regular (13, 12)-lattice. **f** After a sharp increase of irregularity in the fronts from 1 to 36, and a phase of wild oscillation as the parastichy number difference remains relatively high, the fronts become increasingly regular.

simultaneously on both sides (left for red, right for green), as during the diameter reduction. But a series of red pentagons appears close to the red triangles, canceling their effect, while there are still green triangles appearing. This induces a growing difference between the parastichy numbers (Fig. 13c). Finally, the green pentagons appear, canceling the effect of the green triangles. During this crisis, the irregularity of the front (Fig. 13f) fluctuates but globally decreases. After the crisis, at around Iteration 150, parastichy numbers stabilize above the ones reached at the end of the diameter decrease. This is coherent with the triangle transitions happening right after the diameter stabilization, showing that there is a kind of delay between the diameter decrease and the formation of the triangles. The crisis comes from the fact that the large irregularity created too many triangles. From around Iteration 200 on, one observes a final, slow stabilization with few triangle–pentagon pairs and the parastichy numbers oscillating around the final values of (13, 12), when the pattern has converged to a rhombic tiling. During this last convergence phase, irregularity in the last three plateaus of the pattern (between the local peaks due to triangle–pentagon pairs) continues to decrease: irregularity is 0.447394, 0.446905, 0.446679 at Fronts 500, 600, 800, respectively. This shows that these triangle–pentagon pairs, in a concentrated way first and then sporadically, regularize the pattern.

Although seemingly chaotic, the resultant vector plot strikingly illustrates the different phases of transitions of this pattern. In the first phase (in orange) of rapid diameter decrease, triangle transitions create the characteristic butterfly-like asymmetry:

green triangles push the resultant north-east while red ones push it north-west, while in rhombic transitions, the decrease in diameter brings the resultant down. This pattern becomes somewhat dampened as the increasingly small triangles have less influence on the change of the resultant. This dampened oscillation and the simultaneous occurrence of triangles on both sides bring the resultant closer to the center in an erratic way reminiscent of the trajectory of a fly. After the diameter stops decreasing (blue plot), a series of green triangle transitions, combined with a relatively smaller number of red transitions, pushes the resultant north-east. That push is then dampened by pentagons that bring the resultant back toward the center, close to the intermediate circle (in dashed beige) which is the locus of resultants of square lattices fronts. The final series of red pentagon/triangle transitions [as visible from the parastichy numbers graph (Fig. 13c)] results in the repeated oscillations of the resultant along the NW–SE axis. A closer look would show the resultant approaching the NW boundary of the (13, 12) cell, sign of the regularization of the pattern: this boundary corresponds to fronts with equal down-vectors. The larger blue point marks the end resultant, common to all fronts above the last red pentagon, at Iteration 721, when the pattern has settled into a rhombic tiling.

It is also interesting to note that in this pattern the mean divergence angle decreases almost monotonically while the diameter is decreasing, but starts to be very noisy at the beginning of the constant diameter growth phase. The latter is due to the wildly varying parastichy numbers of the fronts as the pattern is transitioning. In the regularizing phase, the mean divergence angle stabilizes as soon as the parastichy numbers are also stabilized (after roughly Iteration 150), even though it fluctuates slightly with the last triangle–pentagon pairs. This shows that the last, isolated triangle/pentagon pairs are there only to reduce the irregularity of the front, which decreases noticeably. They continue having a small fluctuating effect on the local parastichy numbers, but this effect is dampened in the mean divergence angle by taking an average over the front.

The Fibonacci and the quasi-symmetric transitions scenarios

The characteristics of the parastichy numbers graph of Fig. 12b provide a benchmark for transitions that go "according to plans", yielding Fibonacci phyllotaxis along the way. It sums up graphically the transition scenario that van Iterson drew, for instance (Tab. XIII in [3]). This section spells out these characteristics, shows their prevalence in simulations when conditions of regularity of the initial front and speed of transition are satisfied.

Interestingly, when this scenario breaks down, because of either too much irregularity and/or too rapid a reduction of diameter b, it is most often replaced by the convergence toward a quasi-symmetric state where, as Fig. 13 shows, the parastichy numbers increase monotonically while remaining close to each other. Furthermore, when the diameter is stabilized, the pattern moves away from the symmetry but finally is driven back to it. This shows that, even at constant diameter b, there is a driving force pushing toward quasi-symmetric patterns when fronts are irregular enough.

We can look at transitions at three different geometric scales: those enacted by single primordia (quadrilateral, triangle, pentagon transitions), the medium scale where single transitions organize in a coherent way (e.g., Fibonacci-like transitions where all the possible triangle transitions of a given color in a front are exhausted), and finally the more global view where (hopefully coherent) transition phases occur in succession. We now spell out the two main kinds of mid scale transitions.

Fibonacci transitions and monotone Fibonacci transitions

The Fibonacci transitions as observed in Fig. 12b in the previous section, can be reduced to a simple criterion for each mid-scale transition: *one has a monotone Fibonacci transition when parastichy numbers increase fully on one side* (*up or down*), *while the other side does not change*.

More precisely, say we start with an (m, n)-front with $n < m$ (reverse the role of m, n, and up, down if $n > m$). A monotone Fibonacci transition takes place if a triangle transitions occurs for each m up-vectors, for a total of m triangle transitions, while no other transition takes place. This yields a net addition of m down-vectors, and no change in the number of up-vectors. Hence, the parastichy numbers go from (m, n) to (m, $n+m$). Note that $n + m > m$, and so the roles of the up- and down-vectors are now reversed, ushering a possible monotone Fibonacci transition on the opposite side.

Note that we are talking about generalized Fibonacci transitions. The resulting parastichy numbers (m, $n+m$) might not be Fibonacci numbers if the initial pair (m, n) is not. Plants offer many examples of such transitions according to Fibonacci-like sequences, for instance when they follow the Lucas sequence 1, 3, 4, 7, …, or are bijugate (2, 2, 4, 6, 10, …).

As we will see later, monotone Fibonacci transitions are favored when the fronts are regular enough, that is, when in each front the up-vectors are not too far from being equal to each other, and likewise for the down-vectors. In that case, the side (up or down) of higher parastichy numbers corresponds to the vectors which are more horizontal. Monotone Fibonacci transitions are then a consequence of the local rule of triangle transitions on this regular state: they occur on the most horizontal of the two notch vectors.

"Monotone" means that during a monotone Fibonacci transition there are only triangle transitions and the parastichy numbers can only increase (or stay put). In less regular situations, one observes triangle–pentagon pairs during a transition, making the parastichy numbers oscillate, while the net increase of parastichy numbers is the same as in a monotone Fibonacci transition (see Point A in Fig. 15 and Points P and Q, for $c = -0.03$ in Fig. S3 in Appendix S2). This leads to a weaker definition: *one has a Fibonacci transition when*, *starting from an* (m, n)*-front* (*with say*, $m > n$), *one arrives at an* (m, $m+n$)*-front while the number m of up-vectors stays constant* (*reverse the roles of m and n if* $m < n$).

Clearly a monotone Fibonacci transition is also a Fibonacci transition. But while we can give reasons why, and conditions under which, monotone Fibonacci transitions must occur (see "Heuristic arguments for MGRS and QSS" section), it is much harder to do so for the more general Fibonacci transitions. In a sense, the set of monotone Fibonacci transition are like the harder skeleton of the fuzzier, larger set of Fibonacci transitions. However, these two modes (monotone and not) are hard to distinguish botanically: primordia are not exactly disks and they expand in the space available to them, bridging the small gaps of what would be the pentagon in a pentagon–triangle pair. The observer is left with analyzing contacts of botanical organs, and has to decipher the original packing situation from the different contact lengths (see Part II of this article [23]). The lack of precision in this process allows one to overcome the presence of many triangle–pentagon pairs. This lack of precision shows that the existence of Fibonacci transitions is more robust (as seen in numerical simulations and possibly plants) that can be easily argued for mathematically.

Simultaneous transitions

When a pattern with decreasing b does not follow a Fibonacci transition, one could expect that irregular or random parastichy number patterns occur. But what we observe is that they tend, by and large, to the a new quasi-symmetric type shown in the example above, with parastichy numbers close to one another. Defining precisely quasi-symmetric transitions and determining rigorously the conditions of their occurrence is more difficult however. We define them in opposition to the previous case: *one has a simultaneous transition when the increase of parastichy numbers occurs simultaneously on both side*.

"Simultaneous" in this case means: during the same mid-scale transition time. More precisely, a Fibonacci transition on one side of an (m, n) pattern, with $n < m$ would undergo a full m transitions on the m up-vectors, increasing the down-parastichy numbers from n to $n+m$, without any transition on the n down-vectors. In a simultaneous

transition on a similar front, a triangular transition on a down-vector would have to occur before all the m transitions on the up-vectors have taken place.

Note that the parastichy numbers after a simultaneous transition might differ from that of a Fibonacci transition by only one unit in a direction. While this does happen [see, e.g., Fig. 14 (GRS), the green parastichy number near Primordium 110], our experience is that most patterns undergoing simultaneous transitions tend to bring their parastichy numbers much closer together, in a quasi-symmetric state.

Golden-ratio and quasi-symmetric scenarios (GRS and QSS)

Fibonacci (monotone or not) and simultaneous transitions can be distinguished on relatively short periods of growth. During longer time interval one can observe pure dynamical modes, where only Fibonacci transitions occur, or where only simultaneous transitions occur. There can also be mixed modes, exhibiting one type of transitions during stretches of time followed by the other type.

Two types of convergence. One way to visualize the long term trend of pure states is to take the quotients of the highest parastichy number over the lowest (Fig. 14b). The GRS pattern has only Fibonacci transitions – except for a regularizing pair of triangle–pentagon starting at around 110. The plateaus of constant parastichy numbers (outside the transitions) correspond to pairs of successive Fibonacci parastichy numbers. It is a well known fact that the quotients of successive numbers in Fibonacci-like sequences tend to the golden ratio $\varphi = (1 + \sqrt{5})/2$. Hence, the quotients of the parastichy numbers on these successive plateaus tend to φ, as is clear on Fig. 14b.

In the resultant representation (Fig. 14c) the convergence to the golden ratio takes the form of a butterfly wings pattern converging to the circles given by $||\boldsymbol{R}|| = \varphi||\boldsymbol{R}'||$ and $||\boldsymbol{R}'|| = \varphi||\boldsymbol{R}||$[9].

As we have said before, patterns undergoing only Fibonacci transitions have parastichy numbers following a Fibonacci-like sequence. However, for all Fibonacci-like sequences, the ratio of the successive elements tends to the golden ratio φ[10]. Hence, all the patterns with Fibonacci transitions show convergence to the golden ratio in their quotients of parastichy numbers, and converging butterfly wings in their resultant plots.

This motivates the following definitions: *one has a golden-ratio scenario* (*GRS*) *when after some time one observes only Fibonacci transitions*. *One has a monotone golden-ratio scenario* (*MGRS*) *when after some time one observes only monotone Fibonacci transitions*.

Hence, a MGRS pattern exhibits periods of triangle transitions, all on one side (up or down) until they are exhausted with periods of only quadrilateral transitions separating the all up and all down triangle transitions. The GRS pattern may exhibit some pairs of pentagon/triangle interspersed in the process – but of consistent color.

As for the other type of transition pattern represented by the blue graph in Fig. 14, note that it has no plateaus, and no Fibonacci transitions. This motivates the definition: *one has a quasi-symmetric scenario* (*QSS*) *when after some time one observes only simultaneous transitions*.

The QSS orbit in the figure has another important feature: its quotients of largest to smallest parastichy numbers seem to tend to the constant 1. This can be explained by a bounded difference between the parastichy numbers while they grow. The mathematical archetype for this is the simple limit $\lim_{n\to\infty} (n + c)/n = 1$. This raises the interesting questions:

---

[9] Indeed, for the front of a lattice of parastichy numbers (m, n), we must have $||\boldsymbol{R}||/||\boldsymbol{R}'|| = mb/nb = m/n$ which tends, alternatingly, to φ and $1/\varphi$ as m, n are successive elements of Fibonacci-like sequence increasing to infinity. Simple algebra shows that these circles have equations $(x + a)^2 + y^2 = 1$, where $a = -\varphi$ or $a = 1/\varphi$.

[10] It is a known fact that any sequence which is solution of a (Fibonacci) recurrence relation $\boldsymbol{u}_n = \boldsymbol{u}_{n-1} + \boldsymbol{u}_{n-2}$ with initial conditions $\boldsymbol{u}_0 = a$, $\boldsymbol{u}_1 = b$, the ratio $\boldsymbol{u}_n/\boldsymbol{u}_{n-1}$ tends to the golden ratio φ as n grows large, regardless of the initial conditions of positive integers a, b. A shortcut to see this is, assuming $\boldsymbol{u}_n$ has a limit L, $\boldsymbol{u}_n = \boldsymbol{u}_{n-1} + \boldsymbol{u}_{n-2} \Rightarrow \boldsymbol{u}_n/\boldsymbol{u}_{n-2} = \boldsymbol{u}_{n-1}/\boldsymbol{u}_{n-2} + 1$. Taking the limit, one obtains $L^2 = L + 1$, which has solution the golden ratio (and a negative number irrelevant here).

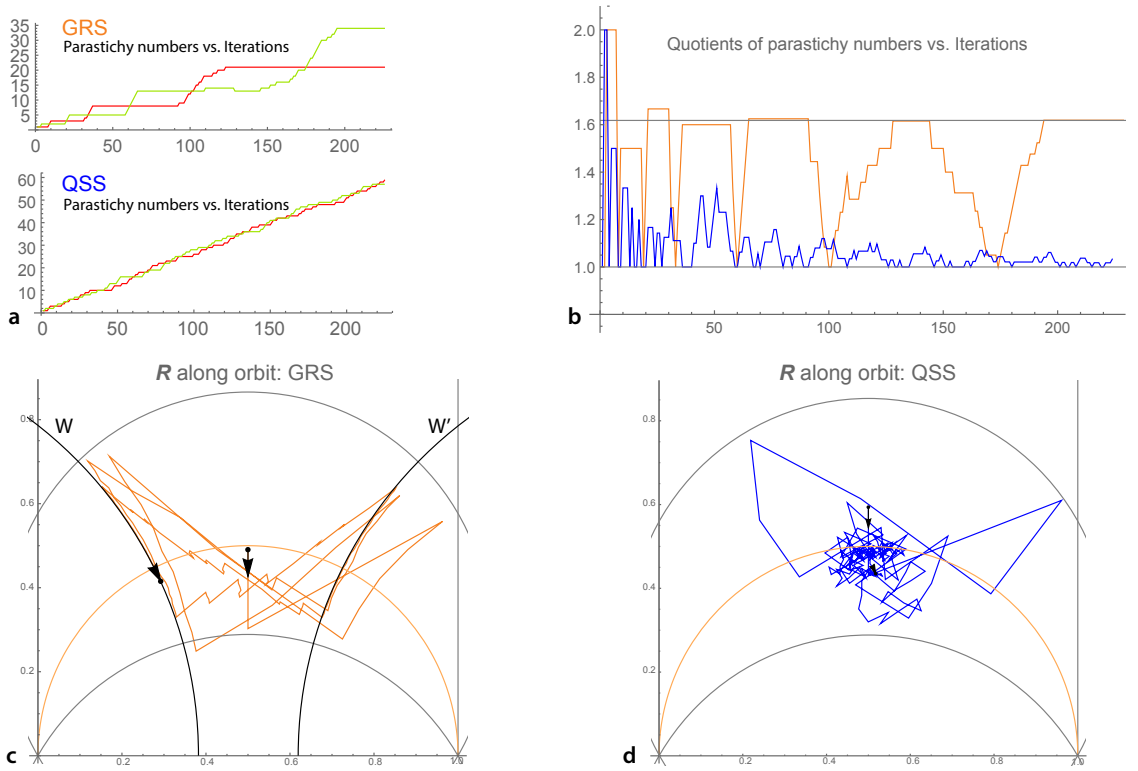

Fig. 14 Two types of convergence. **a** Parastichy numbers of successive fronts in the simulations of Fig. 11 (GRS) and Fig. 13 (QSS), where we kept the radius decreasing at the same initial rates over 225 iterations. **b** We plotted the ratios of the largest parastichy number over the smallest along the orbits from the left. The plateaus of the orange graphs tend to the golden ratio φ, as quotients of successive Fibonacci numbers. The blue graph tends to 1 since the difference of the parastichy numbers stays bounded while the numbers grow. **c** Resultant plot of the GRS orbit. The "butterfly wings" converge to the circles W given by $||R'|| = \varphi||R||$ and W′ by $||R|| = \varphi||R'||$. **d** The QSS resultants produce a "fly flight" pattern, concentrating on the symmetric center $||R'|| = ||R||$, close to the square pattern.

- Do all QSS pattern have quotients of parastichy numbers tending to 1? And, importantly:
- Do the GRS and QSS modes describe the long term behavior of all possible patterns with decreasing disk radius? If not, what other behaviors can there be?

We will return to these questions in section "Heuristic arguments for MGRS and QSS", after having gathered more information about these two types of patterns.

Note that, the resultant graphs both tend to symmetric patterns: for QSS, it is the trivial symmetry of a point central to the resultant plane. For GRS, it is a butterfly with symmetric wings on the arcs of circles defined by the golden ratio.

Sweep through the set of (1, 1)-fronts with varying radius decrease rate

To explore the respective domains of applicability of the golden ratio scenario and the quasi-symmetric scenario, we simulated the disk-stacking process, sweeping through a comprehensive sets of initial (1, 1)- and (2, 2)-fronts (representing the monocot, and dicot, initial conditions in plants [see Appendix S2 for the (2, 2) case]. We decrease linearly the diameter b of the disks with their height h: $b(h) = b_0 + ch$, $c \leq 0$. In the (1, 1) case, we swept the linear rate of decrease c through the interval $[-0.28, 0]$, and the initial diameter b_0 through the interval [0.5, 1] (or [0.25, 0.5] for the radius) in the initial (1, 1)-front – thus covering entirely the possible set of these fronts. We assumed that the two initial disks have equal size. We stopped the simulation the step before the front had reached a prescribed length of 22. To classify the patterns we:

1. recorded the last pair of parastichy numbers,
2. used an algorithm to detect configurations that did follow the MGRS (see Appendix S1),

3. measured the mean over the trajectory of the quotients of the largest parastichy number over the smallest,
4. computed the irregularity of the first front of length 3.

The information for Item 2 in the previous list is represented graphically in Fig. 15a, the one for Item 3 in Fig. 15b, and Item 4 in Fig. 16.

These sweeps confirm the prevalence of MGRS configurations starting with (1, 1)-fronts when the first front of length 3 (that is the first (1, 2)- or (2, 1)-front) in the configuration is regular enough, and the speed of decrease is not too large. We note however some significant "outposts" of the MGRS for larger rates of decrease. Reciprocally, when the initial front of length 3 is too irregular, and/or the speed of transition too large, we observe the predominance of the quasi-symmetric scenario. Conditions of speed and regularity are linked since a quick decrease of diameter creates irregular fronts.

The situation with configurations starting with (2, 2)-fronts is a little more subtle, but still exhibits the correlation between regularity of early Fibonacci fronts, the relatively slow decrease of diameter, and the MGRS scenario (see Appendix S2).

Quasi-symmetric scenario vs. golden-ratio scenario. To detect the quasi-symmetric modes numerically, we computed, for each front of parastichy numbers (m, n) the

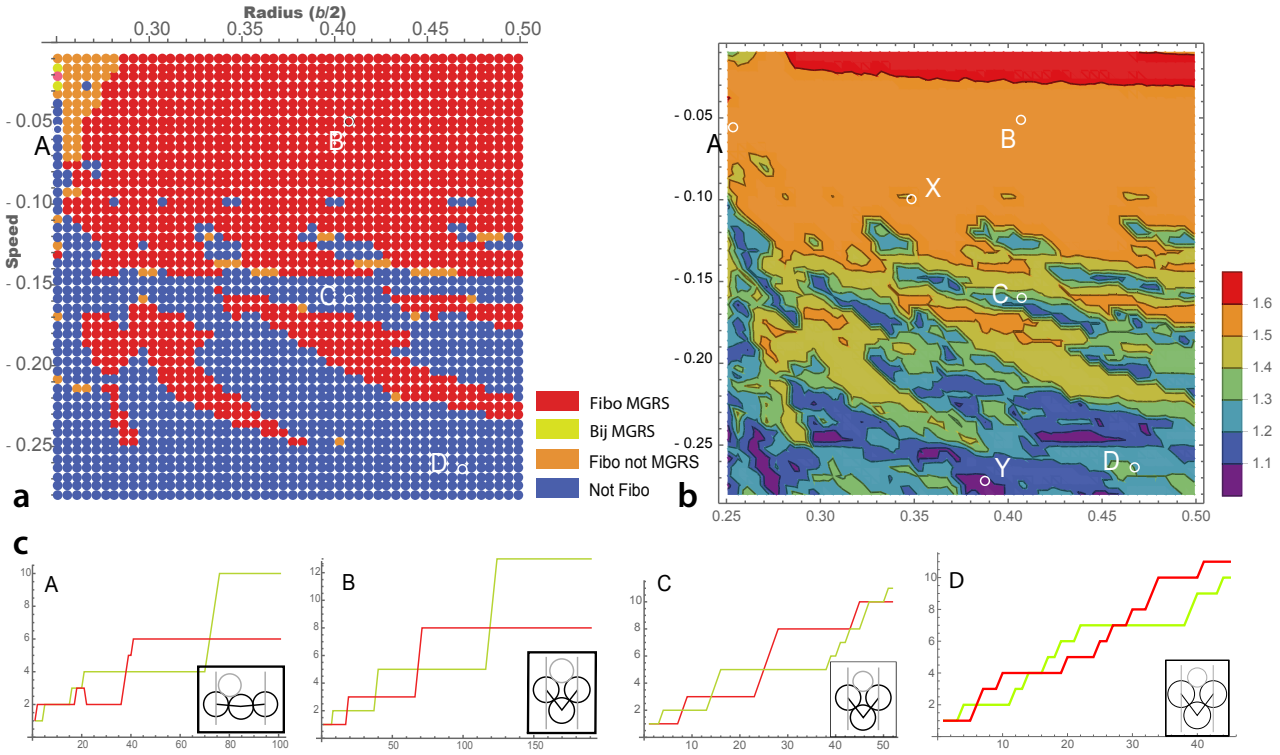

Fig. 15 The MGRS and QSS scenarios on (1, 1)-fronts. **a** The horizontal axis denotes all possible radii of the disks in an initial (1, 1)-front. The vertical axis is the linear rate of decrease of the radius, as a function of height. Points in parameter space are colored in red if the corresponding configurations follows the MGRS, in orange if their last front is Fibonacci, in yellow if they are bijugate and MGRS, and in blue otherwise. Note the predominance of MGRS for smaller speeds and large enough radius (top right of the parameter space). Four points in the parameter space are singled out with the corresponding starting fronts and parastichy number graphs shown in panel **c**. **b** Plot, in the same parameter space as in panel **a**, of the mean quotient of the higher parastichy number over the lower. The bluer regions correspond to mean quotient closer to 1, a sign of QSS, while the redder regions have mean quotient closer to $\varphi = 1.618\ldots$, corresponding to MGRS. Note the correspondence between panel **a** and **b**. Aside from the four Points A, B, C, and D marked in panel **a**, we added the Points X and Y corresponding to the simulations of the MGRS and QSS patterns studied above. **c** Point A: bijugate configuration, ending with parastichy numbers (6, 10). The beginning can be seen as a QSS, followed by the separation of the parastichy numbers, and a pure MGRS. Note the decrease of the down- (red) parastichy number at Iteration 20. A pentagon must have occurred there, breaking the monotonicity. Point B: MGRS configuration ending in (13, 8)-fronts. Point C: a configuration that follows Fibonacci transitions till its 38th iteration and then shifts to QSS: zones of transitions overlap. Point D: a pure configuration of QSS. Note the small spread between its parastichy numbers.

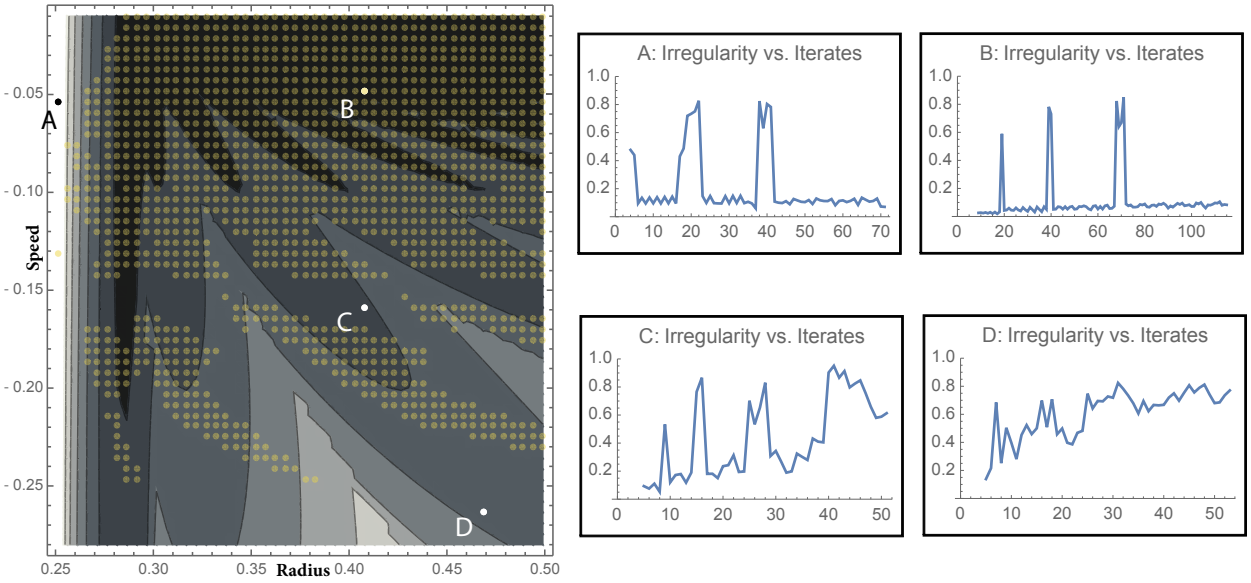

Fig. 16 MGRS/QSS vs. regularity. On the left, in the background, the contour plot of the irregularity function of the first front of length 3 encountered in configurations starting as (1, 1)-fronts. The plot region is the same (radius, rate of decrease) as for the sweep in Fig. 15. The darker regions correspond to greater regularity. The MGRS points are superimposed (in transparent yellow) to the plot, more present in the darker regions: evidence that regularity correlates with MGRS, especially at low speeds. On the right, the irregularity of the successive fronts corresponding to the initial radius and rate of decrease of the four points marked on the left. Note the substantially higher and increasing baseline irregularity for Points C and D, and the (expected) spikes of irregularity at the triangle transitions.

quotient $\max(m,n)/\min(m,n)$ of the largest parastichy number over the smallest. We then took the mean of that quotient over all the fronts in a pattern, excluding the first 20 (to better capture the asymptotic trend). As mentioned before, any pattern following the GRS (regardless of its initial condition) has, away from transitions, this quotient tending to the golden ratio.

The pattern not following Fibonacci transitions inevitably have smaller quotient. Indeed, in the second phase of a Fibonacci transition, when the small parastichy number overcomes the large one, it continues growing while the other stays put, creating the largest possible distance between the two numbers. But in simultaneous transitions, the other parastichy number does not stay put and increases as well, diminishing the distance between the two numbers.

Fig. 15a,b, with the blue regions of low mean quotient mirroring the blue regions of non MGRS, provides visual evidence to our assertion that non MGRS patterns tend to be QSS.

MGRS/QSS vs. regularity. In Fig. 16, some of the structure of the contours of the irregularity function echoes the structure of the MGRS data. The MGRS points tend to congregate in the darker regions of greater regularity; reciprocally, the QSS points gather around the areas of greater irregularity, and/or greater speed. Indeed, most MGRS points are confined to regions of irregularity less than 15%. In other words, the regularity of the initial front of length 3 is a good predictor of further regularity of the fronts (aside from transitions period) and of the monotonicity of the pattern. This correlation becomes weaker at higher speed of decrease, in the bottom of plot. Again, this is not too surprising: faster decrease brings more disorder, and the influence of the initial conditions fades away more quickly. So early regularity is less predictive of long term behavior as it is at lower decrease speed.

Greater regularity is seen in the upper right corner of the picture, for greater radius. This could be expected: the transition to a front of length 3 is immediate for configurations of smaller initial radius (to the left), but may not yield a regular front. For instance, at Point A, the initial front is essentially flat, yielding a triangle transition in the first iteration (Fig. 15c). One of the up-vectors of the resulting (2, 1)-front is essentially horizontal, and is far from parallel to the new up-vector, which is the side of an almost equilateral triangle with almost horizontal base. On the other hand, when

the radius is large enough (larger than $1/2\sqrt{3} \approx 0.29$ for small speed), the notch angle is small enough (less than 120°) to afford a quadrilateral transition. When that's the case, for small rates of decrease of the radius, the fronts have their notch angle open progressively to a value close to 120° where a triangular transition yields an almost equilateral triangle with a side almost parallel to the remaining notch vector, hence preserving regularity and setting the MGRS in motion.

The structure of the irregularity plot, and in particular its self-similar aspects, is further explained by the number of iterations that it takes to reach a front of length 3 in each simulation. The dark tongue on the left correspond to initial fronts whose notch angle is close to 120°. The other tongues correspond to fronts whose second, then third, etc. iterations have angles close to 120°. These latter tongues veer right since it takes less iterations to reach the transition angle when the radius decreases faster. See Fig. S1 for more evidence of this. These self-similar structures are also visible in the GRS/QSS regions in Fig. 15, evidence that low irregularity plays an important role in the MGRS.

Heuristic arguments for MGRS and QSS

Why Fibonacci?

The simulations we have performed indicate that a combination of initial front regularity and low speed of diameter decrease make the monotone golden-ratio scenario robust. This brings us to the following simple heuristic argument for the prevalence of MGRS, spelling out where the condition of slow decrease and regularity may be needed.

1. Start with a regular enough front with parastichy numbers m, n. Assume $m > n$ (more up- than down-vectors – the case $n > m$ is identical).
2. Assume the notch angles of the front are not too close to 120°, and that the speed of decrease of the disk diameter b is not too high.
3. Because of the low speed of decrease of b, the quadrilateral transitions are almost rhombic and transform the front vectors into similar front vectors, preserving the regularity of the front.
4. The vectors are becoming more horizontal because of the decreasing diameter b, and the notch angles are becoming wider, ushering triangle transitions (this corresponds to the decrease of the resultant vector along the border of the "butterfly wing" as in Fig. 14).
5. Because of regularity, each of the m up-vectors is more horizontal than any of the n down-vectors. The triangle transitions must then occur on the up-vectors.
6. Since b decreases slowly, the triangle transitions occur on notches whose angles are close to 120°, and each of these triangles is close to equilateral.
7. An almost equilateral triangle transition on the up-vector of a notch of almost 120° yields an up-vector almost 60° steeper, and a new down-vector almost parallel to the down-vector of the notch.
8. Both of the new vectors are steeper than the original up-vectors of the front, and will not host a triangle transition.
9. When all the original up-vectors are spent in triangle transitions, the m up-vectors are replaced by m up-vectors roughly 60° steeper, and m new down-vectors are added, that are similar to the n original ones (this corresponds to the full shift from the bottom of one butterfly wing to the top of the wing on the other side in Fig. 14).
10. The new $(m, n+m)$-front has kept enough regularity, the notch angles are around 60° (far from 120°) and the process is ready to start over again.

This heuristic argument does not presume that the original front is Fibonacci. It could be a (1, 3)-front, yielding Lucas phyllotaxis, or (2, 4), yielding bijugate phyllotaxis or another type of front leading to a more exotic sequence.

Note also that, in the last step, we mention the notch angles being close to 60°. If they are too close to that angle, there can appear pentagons (see Fig. 7) which, with

an otherwise regular front, usually yields a triangle/pentagon pair. This breaks the monotonicity of the process, and makes a MGRS into a GRS. But at the same time, as we have seen, triangle/pentagon pairs tend to regularize the pattern, making even the non monotone GRS robust. This phenomenon can be observed in the patterns at Points P and Q of Fig. S3.

Toward quasi-symmetry?

In the simulation of Fig. 13, we saw two ways in which a pattern became quasi-symmetric. The first way occurs in the first phase of the pattern, where the diameter decreases quickly (up to Iteration 36). The triangle transitions are alternating evenly between up- and down-vectors, creating fronts of great irregularity, and parastichy numbers close to one another. No pentagon transition takes place during this phase.

The second way shows as a slower drift toward quasi-symmetry, with a combination of triangle and pentagon transitions. This happens in our pattern, in the constant diameter phase, after a period of adjustment where the parastichy numbers first grow apart (up to (17, 11), a healthy asymmetry, at Iteration 76). This shows two types of convergence toward quasi-symmetric parastichy numbers, one with rapid decrease of the diameter, and the other at constant diameter but large irregularity.

QSS at rapidly decreasing diameter. QSS (see Fig. 14) relies on the strong irregularity as created by a quick reduction of diameter b. A first interpretation of this behavior is that as the reduction of b is very quick, the notch angles become flat and allow for triangular transitions all along the front, irrespective of the direction (up or down). The front flattening effect of the fast decrease of b is so strong that it trumps, locally, the considerations as to which side (up or down) has more vectors. A first interpretation of quasi-symmetry is then that the flattening effect leads to a symmetric state. One could call this a "passive" symmetry.

That parastichy numbers of QSS patterns should be closer together than in GRS patterns is almost tautological. In the second phase of a Fibonacci transition, after the smallest parastichy number has overcome the largest one, it continues growing while the other stays put, creating the largest possible distance between these two numbers. But in simultaneous transitions, the other parastichy number does not stay put and increases as well, diminishing the potential distance between the two parastichy numbers. This can be seen in Fig. 14, where the GRS pattern ceases to be strictly GRS for a moment because of one simultaneous transition at around Iteration 110: the parastichy numbers differ by one less than they could.

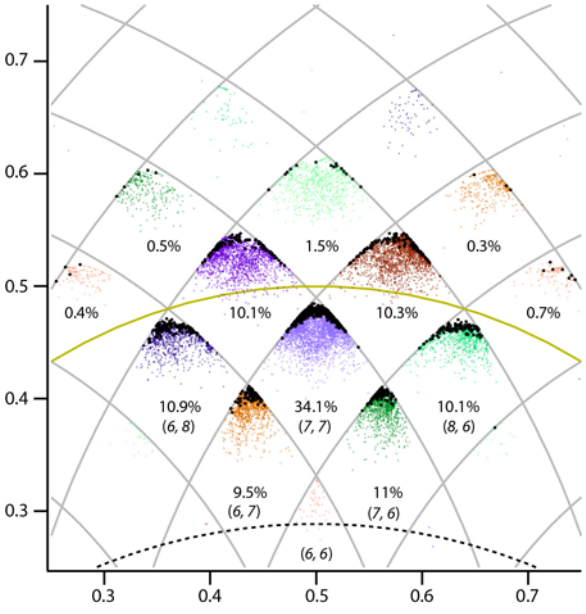

Fig. 17 Drift from irregular (6, 6)-fronts toward nearly square (7, 7)-rhombic tilings. Starting from a thousand initial (6, 6) states with very irregularly placed initial primordia, this figure shows, in a rectangular region of the cylinder, the resultant vector for the intermediate fronts (in different colors for each cell), and the resultant of the final rhombic tiling front in black. The respective percentage of final resultants in each region are also indicated.

Drift toward the center at constant diameter: (6, 6) initial conditions. To further check the role of irregularity in transitions, we isolate it from the effect of diameter decrease, and perform many simulations with a constant diameter b, on random fronts close to a triangle transition [with a resultant in the lower triangular (or 120°) limit; Fig. 17]. Adding some irregularity makes the pattern undergo series of transitions, until they eventually stabilize into rhombic tilings (the fact that they always do stabilize is the point of a paper to come, by Golé and Douady). When looking a the final resultants of the patterns, we see that they are mainly in the central region, corresponding to rhombic tilings with symmetric parastichy numbers ((7, 7) in our experiment), and tiles close to square in average. This is, qualitatively, not surprising given the initial equality of parastichy numbers. But looking at the percentages of final resultants landing in the different parastichy numbers cells indicates a drift to the center which cannot

solely be explained by the symmetry of the initial conditions. Indeed, if up or down triangular transitions were randomly chosen, one could deduce the proportions of the percentages for patterns that underwent two triangular transitions from the number of possible routes leading to them. In our example, the relative proportions of the percentages in the (6, 8), (7, 7), and (8, 6) cells should be 1/2/1, as in a Pascal triangle, as there are twice the number of transition routes between (6, 6) and (7, 7) as there are between (6, 6) and (6, 8) or (8, 6). But instead, we observe a proportion close to 1/3/1. In the cells necessitating three triangle transitions from (6, 6), that is the cells (6, 9), (7, 8), (8, 7), and (9, 6), the phenomenon is even clearer: the number of possible routes would predict 1/3/3/1 proportions, while we observe 1/19/19/1.

Drift toward the center at constant diameter: (5, 8) initial conditions. To confirm that the symmetry of the initial condition is not entirely responsible for the drift toward the center, we performed another experiment (Fig. 18). We started this time with random fronts with Fibonacci parastichy numbers (5, 8) at a value of the diameter b corresponding to that of the (5, 8)-square lattice. That is, we chose fronts which, on average, were far from symmetric and as far away from any transition as possible. We colored the (tip of the) resultant of the initial fronts according to their regularity [yellow (regular), blue (irregular), red (very irregular)], and ran the disk-stacking process long enough to approach convergence. We colored the resultant of each final front with the same color as its initial one. With sufficiently large irregularity, the notch angles can be close to 60° or 120° and transitions can, and do, occur. The resultants of the final fronts present a clear drift toward symmetry in their parastichy numbers: while most of the front with yellow initial resultants stay in the (5, 8) cell, most of the irregular ones land in cells to the right of the (5, 8) cell. Those that eventually land to the left (e.g., (4, 8)) seem to be predominantly red (very irregular). One can also observe a drift to a square state in the results of our simulation: a tiny proportion of fronts ended up in the (7, 8) cell, compared to the very populated (6, 7), which is closer to the circle of resultants of square lattices. Hence the patterns converge to rhombic tilings that tend to be, on average, more square.

Explaining quasi-symmetry when the diameter decreases. As we said above, it is tautological that in simultaneous transitions, the parastichies numbers are staying close together as they both increase during the same period of time. But simulations (as in Fig. 13) point to other interesting phenomena. Indeed, while the transitions maybe simultaneously on up- or down-vectors, the two types of triangles remain partly segregated spatially. It seems that the coherence (only red or only green) is preserved locally, making (spatially) local Fibonacci transitions that are also roughly alternating in time, from one color to the other. The decrease of b creates some spatial differences in

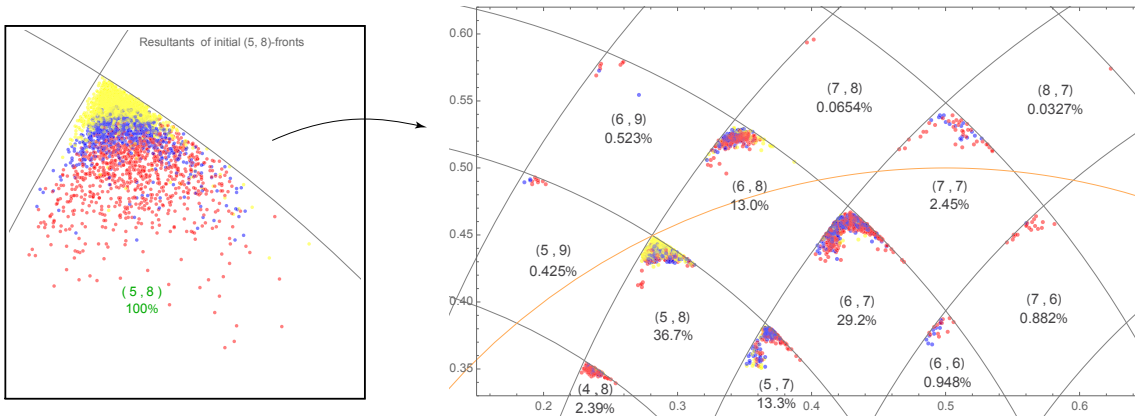

Fig. 18 Drift from Fibonacci to symmetric fronts. Starting from more than a thousands randomly picked initial (5, 8)-fronts we applied the stacking process with constant radius to them. Left: the resultant of the initial front, colored according to three ranges of regularity: regular (yellow), irregular (blue), very irregular (red). Right: the resultants of the iterates of the front whose resultants are on the left, after many iterations, each colored in the same color as its initial front. Note the drift towards the center (the orange arc of circle is the locus of resultants of fronts of square lattices).

the shape and regularity of the fronts. If the decrease is slow, these differences propagate along the two parastichies directions before the next transition front is reached. But if the speed of decrease is large, these differences impact directly and locally the next transitions. The differences then may remain in coherent zones. When the width of these zones is smaller than half the circumference (just as in Fig. 13), it ensures that the transitions in both directions appear simultaneously (with our previous definition of simultaneity). This maintains near-equality of the parastichy numbers. The question is then: how does the size of the coherent zone evolve with the iterations? If we follow the same logic as above, then more irregularities should appear and break the coherent zones into smaller pieces, increasing the mixing.

Explaining the drift toward symmetry at constant radius. We discuss how irregularity can explain the drift toward the center seen in the two previous experiments. Irregularity triggers many transitions, when front notch angles are pushed to the 120° or 60° limits, either directly or after permutations of front vectors induced by rhombic transitions. There is a certain asymmetry in these transitions however. Pentagon transitions occur on front notches of three vectors (two down, one up, or one down, two up), and the outcome is a vector of each type (one up and one down). But in general, a pair of two adjacent vectors of the same type is more likely to occur in a front where there is more vectors of that type than the other. Hence, the side of the notch with two vectors corresponds, in general, to the side with greater parastichy number in the front. Hence, in general, a pentagon transition on a front decreases the largest parastichy number (see Fig. 10 in Part II [23]). Similarly, as we have argued for the Fibonacci case, triangle transitions will tend to occur more on the vectors of higher parastichy numbers, as they tend to be more horizontal. This has the effect of increasing the smaller parastichy number of the front. *These two effects combined bring the two parastichy numbers of the front together*.

Explaining the drift toward square packing at constant radius. As for the convergence toward the more square rhombic tilings, irregular fronts whose resultant are closer to the 120° (triangle) or 60° (pentagon) transition boundaries will tend to transition away from the boundary. The more irregular the front, the more likely that one of its notches reaches the angle conditions triggering a transition. And such a transition pushes the resultant of the front up from the triangle boundary, and down from the pentagon boundary, in either case closer to the center (see Fig. 14). On the other hand, the fronts with resultants closer to the line of square lattice resultants are the least prone to transitions. Thus, the instability of fronts with resultants in the upper and lower boundaries, and the relative stability of those near the square locus ensure that patterns tend to drift towards that locus, and the more irregular the front, the more pronounced the drift, as evidenced by Fig. 18.

Are there patterns other than GRS and QSS?

In our exploration, we have revealed two scenarios of transitions for disk-stacking patterns when b decreases. Under the GRS scenario, all triangle transitions are spent on one side before some can appear again on the other side. Under the QSS scenario, there is no waiting till one side is spent – triangle transitions of both types happen almost simultaneously. Here, we begin answering the questions stated in section "Golden-ratio and quasi-symmetric scenarios (GRS and QSS)", namely: are there patterns that do not follow either scenario? And even if a pattern follows QSS, does it mean that the quotient of its parastichy numbers must tend to 1?

One possibility that does not quite fit either the MGRS or QSS scenarios is a pattern that displays both. One such instance, which seems to occur quite a bit, is seen in Point C of Fig. 15: a pattern that starts as a GRS and switches to QSS. Intuitively, irregularity may accumulate in the MGRS pattern which makes it switch to a QSS, especially when the relative rate of decrease of diameter increases. Point A of Fig. 15 shows an example of a pattern that does the converse: starting for a few iterations as a QSS (as a (2, 2) and then (3, 3) whorled pattern), then switching to a MGRS. Such cases seem to be limited to early stages QSS: although we have not searched

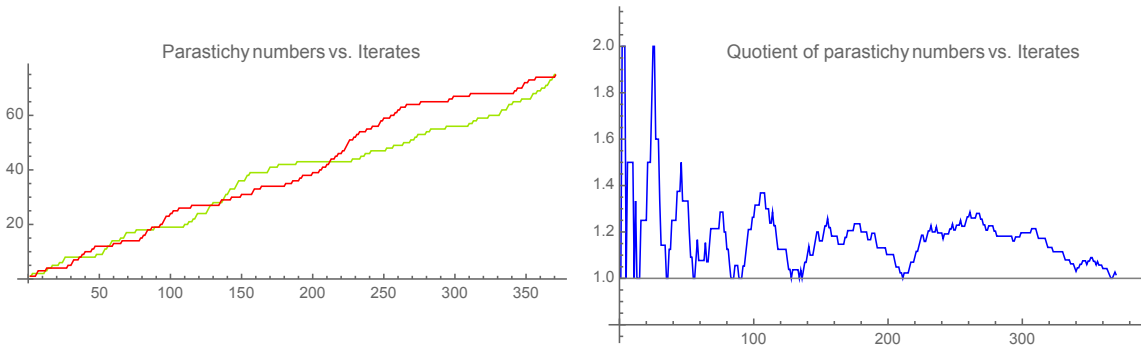

Fig. 19 QSS pattern with unbounded parastichy numbers difference? Note how the green and red graphs seem to oscillate around one another with increasing amplitude. Accordingly, the ratio of the parastichy numbers oscillates without its amplitude seeming to converge to 0.

them systematically, we have not seen examples with a long period of QSS which then switches to GRS. So apart from early symmetric beginnings and late breaking down of GRS, we have not observed identifiable mixed states.

Our example of Fig. 14a shows (timidly) the possibility of a switch and reverse switch: at around Iteration 110, a triangle transitions breaks the monotonicity of the pattern, and its GRS character. In this case, it is neutralized by a pentagon transition within 20 iterations. We have also seen patterns where the quotient of the parastichy numbers although not tending to the golden ratio seems to oscillate without clearly tending to 1 (Fig. 19). The figure indicates that the difference between the parastichy numbers could be unbounded. Accordingly, the quotient of the parastichy numbers oscillates without diminishing amplitude.

In theory, one could imagine patterns that would, after a run of Fibonacci-like transitions, become irregular just so as to drift toward a very regular (n, n) pattern which would then itself undergo a series of Fibonacci-like transitions. One could even imagine repeating this process indefinitely with prescribed lengths in the lapses of GRS and QSS, in a way reminiscent of the Fibonacci iterations in an L-system [42]. Asymptotically, the quotient of the parastichy numbers might approach a slope strictly between 1 and φ. But we would still remain in the duality GRS/QSS. What is harder to imagine is a truly different mechanism yielding the ratio of parastichy numbers tending to such a number.

Our fledgling understanding of the interface between GRS and QSS begs for more studies. But it should not detract from the important duality of these two classes of phyllotaxies stressed in this article. Indeed, one has to remember that plants produce only finitely many primordia. Hence, assigning asymptotic behaviors in the strict mathematical sense to plants might be meaningless. What our work indicates however, is that (***i***) given a total number of primordia, we can ensure that the pattern follows MGRS (or at least GRS) as long as the initial fronts are regular enough and the rate of decrease of b is small enough, (***ii***) for large enough irregularity and large enough rates of decrease, patterns will follow QSS, (***iii***) irregularity yields a drift towards quasi-symmetry, without the need of radius decrease.

These facts are enough to give testable conditions for plants to exhibit one or the other pattern.

Towards a mathematical explanation

As pointed out in the introduction, this paper has tried to stay away, inasmuch as possible, from mathematical technicalities. Nonetheless, we give some very rough sketches here, of some of the underlying mathematical structures behind our results, and ways that some of our heuristic arguments could be turned into proofs. These abstract images have guided us in our explorations.

Clearly, the heuristic argument for "Why Fibonacci?" in the previous section seems to lend itself to a proof by induction of the validity of the MGRS scenario for an open

set of initial conditions and speed of decrease. Apart from providing a solid proof of the existence and robustness of the MGRS, it might point to subtle geometric and dynamical mechanisms that we have not uncovered here. For a more precise mathematical statement, we propose the following **conjecture**:

Given three positive integers n, m, N, there exists a non empty open set of triplets (ε_1, ε_2, ε_3) *of positive real numbers such that, given a front of parastichy numbers n, m whose irregularity is less than* ε_1, *with notch angles less than* $60° + \varepsilon_2$ *and the rate of decrease of the diameter is less than* ε_3, *then the disk-stacking process undergoes N Fibonacci transitions.*

Another, more global mathematical interpretation underlies the disk-stacking model, one that is related to past work based on dynamical systems and the van Iterson's diagram [3,34,36].The disk-stacking process (at constant diameter b for now) can be seen as a discrete dynamical system on a configuration space of large dimensions. We choose to consider a large number N of disks in our configurations and the configuration space is made of the coordinates of the centers of the disks, a space of dimension $2N$. The dynamical system then consists of applying the stacking process on those configurations, adding a disk on top and removing the lowest disk to conserve dimensions [6,43]. In this configuration space, the sets of (m, n)-rhombic tilings are subsets (manifolds with boundaries and "corners") of large dimensions ($m + n - 1$: the degrees of freedom one has in deforming a fronts) [6]. Many of these rhombic tilings, call them the dynamical tilings, correspond to periodic orbits, of period mn. The (m, n)-rhombic lattice of same diameter b is part of this set, and is often a fixed point. The rhombic lattice is also part of the van Iterson diagram [3,5,34]. When the lattice is a fixed point, it is neutrally stable, but not attracting (contrary to the situation in the system studied in [34]). On the other hand, each set of rhombic tilings is itself (strongly) attracting, as we have witnessed repeatedly in this paper: in Fig. 6a, the system converges in a few iterations to a rhombic tiling. Also, what we have called regularization is just a mechanism of convergence toward a rhombic tiling. This set is also dynamically invariant: a front of rhombic tiling can only turn into a front of the same rhombic tiling under the stacking process.

One can think therefore of the MGRS scenario as orbits of a dynamical system of high dimensions hovering around a complicated attractor that contains as its skeleton the van Iterson diagram. Starting with a front close to that of a rhombic lattice in the van Iterson diagram, the strong attraction of the rhombic tilings will ensure that the orbit stays close enough to the successive rhombic lattices of a branch of the diagram as the parameter decreases, and thus the fronts will undergo Fibonacci transitions.

If the speed of decrease of the parameter is too large, the orbit will likely get out of the basin of attraction of Fibonacci rhombic tilings. It must tend to some set of rhombic tilings however. The largest such sets are, for a given length of fronts, and given b, the sets of rhombic tilings that offer room for the largest range of front irregularities. Those must be the most symmetric, most square tilings: they are (in average) the furthest away from transitions. Indeed, these tilings have notch angles, on average, that are farthest away possible from the triangle and pentagon transitions of 120° and 60°. Hence, with more room for perturbation of their fronts, the sets of such rhombic tilings are indeed larger. By extension, their basins of attraction are also larger. Note that if the front of the pattern lands close enough to that of a regular (n, n)-lattice, then a whole new set of Fibonacci transitions could occur, giving a possible mechanism for alternating MGRS and QSS scenarios in one pattern.

The fuzziest part of these dynamical arguments is our inferring properties for the dynamics of the system with varying parameter from the one with constant parameter. One way to clarify this is to think of the stacking process with diameter decrease as a dynamical system in its own right: instead of disks of constant diameter, we make them of diameter varying with height. The configuration space is the same as before (collection of the centers of the disks) but the dynamical rules are different, as it is height dependent. Because of its strong attracting nature, the dynamically invariant set of rhombic tilings for constant b could mutate, in the system with decreasing b, to a nearby attracting invariant set which would conserve some of the geometry and dynamics of the set of rhombic tilings [6,44]. This promises to be challenging to prove rigorously however, since our system is at times multivalued.

Conclusion

In this article, we revisit the dynamical model of disk-packing first proposed by Schwendener [2]. We first show how the local nature of the packing rule allows to determine the strictly necessary information at each time step, encapsulated in the front. We then show how one can measure many local characteristics of the pattern at any time step such as the front parastichy numbers, the resultant vector, the mean divergence angle, the irregularity. We also analyze the local transitions that affect the whole pattern, mostly triangle or pentagon transitions. These tools turn out to be powerful for the study of phyllotactic patterns and their ontogenesis. They could be used in many modeling situations, for instance even when partial differential equations are used to simulate the successive apparition of roughly constant size disks [12], or in analyzing real botanical examples (see [22,23]).

This disk-packing model can be anchored in the findings of modern biology. The end result of the complex mechanisms at play is, as already described by Hofmeister, the production of a primordium of a given size enclosed between the central region and the previous primordia, and away from the most recent primordia. The starting point of the disk-packing model, or of the very closely related iterative potential models [25,38] is thus anchored in this biological reality.

The model looks at its consequences, namely the patterns produced by the iteration of this dynamical system. Since many dynamical models are able to produce similar results based on different mechanisms, geometries, and parameters [11,24,25,34], it means that the occurrence of the phyllotactic patterns is not due to the particularities of the model, or even to the particularities of the underlying biological mechanisms they are supposed to reproduce, but only to the dynamical iteration of the local interactions rules (Hofmeister) that they share. From this, one can expect that new models based on new biological finding [12] will still obtain the same results. The way to sort the models is to look in details at the variety of patterns they can produce, and how closely they can resemble real botanical patterns, and in particular their transitions and irregularities [1]. This is the aim of the second part of this paper [23]. On the theoretical side, analyzing in detail the disk-stacking model with the geometric tools of the fronts and their averages, allowed to expend the usual study of the selection of Fibonacci patterns away from perfectly regular ones into more realistic irregular ones. In particular, we found an argument why, even if considering only local transitions (triangles), and irregular patterns, one can have a global Fibonacci transition, under the condition that the irregularities are not too large and the decrease in primordium size not too quick. Previous arguments were based on global transitions between regular lattice patterns, and thus assumed a much lower range of irregularity. Reciprocally, we show that if the irregularities are too large and the decrease in primordia size too quick, one obtains quasi-symmetric patterns, which are also observed in plants (Part II [23]), even though they are not usually considered in the literature. In view of the overwhelming presence of Fibonacci numbers observed in plants, we can deduce that these developmental conditions are commonly met.

Even though the numerical simulations of "hard" disks can be very similar to the successive addition of soft particles [25], the present explanation of the selection for the Fibonacci numbers is still different from existing ones [3,5,24,34,35,45]. Here, it is not the difference of asymmetry between the two possible new states (usually conflated with lattices) at a packing transition that makes the selection [24,35,45], or careful considerations on the existence or not of these two states at the transition [5,34]. It is rather the asymmetry of the front itself, and its small enough irregularities, that drive directly, and locally, step by step toward the next Fibonacci front. It is our main conclusion that with only local considerations, passing through very irregular states at the transitions, and starting from the simplest initial conditions, the system produces Fibonacci transitions and final Fibonacci number of parastichies. Our explanation is local, dynamical, and robust in presence of irregularities. This makes it, in our view, much stronger than any consideration on regular lattices, or even more so, than any teleological explanation [12].

Such an explanation for the Fibonacci rule and numbers has also the particularity of being inherently simple, and deduced directly from as realistic drawing such as the one of Fig. 3: the most horizontal front vectors support triangular transitions,

increasing the parastichy number in the other direction. Such an explanation can even be conveyed successfully to children (as we have experienced many times ourselves!).

Extending the possible irregularities (and speed of decrease) allowed us to find another type of convergence, toward quasi-symmetric and quasi-square patterns. The convergence toward this kind of state is a new, original finding of this paper. Symmetric states have been long defined in botany as "whorled" phyllotaxis. Except from the work of Snow and Snow [27], spiral phyllotaxis, assumed to be overwhelmingly Fibonacci, and whorled phyllotaxis have been set apart as two distinct families. Here, we find that there are also the outcome of different types of convergence. Thus, our study brings all the possible phyllotactic states together[11]. The existence of nearly symmetric states ((n, n) or $(n, n+1)$) was also obtained in numerical simulations [25], but in a very different way, from a special approach in dealing with empty initial conditions, or from an isolated triangle or pentagon transition with very slow change of diameter. Here, we find these patterns as the result of a robust convergence mechanism from a much more diverse set of possible situations. Our interpretation is also very different. In the simulations of [25], the stability and observation of quasi-symmetric patterns was explained by their globally greater compactness when close to an hexagonal pattern [25] (Fig. 8). However, we found here on the contrary that these quasi-symmetric patterns tend to congregate, as measured by their resultant, close to square lattices, where they are more dynamically stable, away from the local triangular or hexagonal transitions.

The comparison of the stacking model results with botanical observations is the aim of the Part II of this paper, and in a wider scope in a future article. That work confirms the usability of our geometric concepts, and the importance of considering the heretofore barely mentioned quasi-symmetric patterns.

[11] Except the necessary exception, such as *Costus spiralis*. Inspection of its meristem shows that in this case the primordium extend very quickly, surrounding completely the meristem before the next primordium appears. The particular shape of this already grown primordium, leaving more room near its expanded central vein, explains the positioning of the new one, still following Hofmeister principle [38].

Acknowledgments

The authors thank Przemyslaw Prusinkiewicz for his critical and constructive reading of the article. The article benefitted from past work and discussions with Pau Atela. Many students contributed to the Phyllotaxis Lab at Smith College, who implicitly helped with this work. Among others: L. Balay-Wilson, R. Benhart, B. Binet, K. Chau, S. Chen, J. Crouser, G. Diaz, K. Easwar, M. Franz (who used the disk-stacking model to study fast transitions: Franz, M. C. Modeling rapid phyllotactic transitions in *Magnolia* ×*soulangiana* 'Verbanica', 2015, Honors Thesis, Smith College), E. Freeman, L. Grecki (who wrote an early version of the disk-stacking program with varying radius and made interesting simulations: Grecki, L. M. Phyllotaxis dynamics: a study of transitions between plant patterns, 2009, Division III project, Hampshire College), W. Hu, C. Hunter, T. Khendu, A. Lello-Smith, W. Li, C. McGehee, J. Mentor, S. Ostriecher, G. Riggs, E. Rogers, Q. Shen, J. Shin, S. Smith, W. Yu. CG would like to thank Denise Lello, who co-ran the lab, for her priceless intellectual and moral support.

Supplementary material

The following supplementary material for this article is available at http://pbsociety.org.pl/journals/index.php/asbp/rt/suppFiles/asbp.3533/0:

Appendix S1 A meta algorithm for MGRS detection.

Fig. S1 Number of iterations before front of length 3 in (1, 1) sweep.

Appendix S2 Sweep over (2, 2) initial fronts.

References

1. Zagórska-Marek B, Szpak M. Virtual phyllotaxis and real plant model cases. Funct Plant Biol. 2008;35:1025–1033. https://doi.org/10.1071/FP08076

2. Schwendener S. Mechanische Theorie der Blattstellungen. Leipzig: Engelmann; 1878.
3. van Iterson G. Mathematische und mikroskopisch-anatomische Studien über Blattstellungen nebst Betrachtungen über den Schalenbau der Miliolinen. Jena: Gustav Fischer Verlag; 1907. https://doi.org/10.5962/bhl.title.8287
4. Atela P. The geometric and dynamic essence of phyllotaxis. Math Model Nat Phenom. 2011;6:173–186. https://doi.org/10.1051/mmnp/20116207
5. Douady S. The selection of phyllotactic patterns. In: Jean RV, Barabé D, editors. Symmetry in plants. Singapore: World Scientific; 1998. p. 335–358. (Series in Mathematical Biology and Medicine; vol 4). https://doi.org/10.1142/9789814261074_0014
6. Atela P, Golé C. Rhombic tilings and primordia fronts of phyllotaxis [Preprint]. 2007 [cited 2016 Dec 30]. Available from: http://arxiv.org/abs/1701.01361
7. Mughal A, Weaire D. Phyllotaxis, disk packing and Fibonacci numbers [Preprint]. 2016 [cited 2016 Dec 31]. Available from: https://arxiv.org/abs/1608.05824
8. Turing A. The chemical basis of morphogenesis. Philos Trans R Soc Lond B. 1952;237(641):37–72. https://doi.org/10.1098/rstb.1952.0012
9. Veen AH. A computer model for phyllotaxis, a network of automata [Master thesis]. Philadelphia, PA: Computer and Information Sciences Graduate School of Arts and Sciences, University of Pennsylvania; 1973.
10. Williams R. Shoot apex and leaf growth. London: Cambridge University Press; 1974.
11. Meinhardt H, Koch A, Bernasconi G. Models of pattern formation applied to plant development. In: Jean RV, Barabé D, editors. Symmetry in plants. Singapore: World Scientific; 1998. p. 723–758. (Series in Mathematical Biology and Medicine; vol 4). https://doi.org/10.1142/9789814261074_0027
12. Pennybacker M, Shipman P, Newell A. Phyllotaxis: some progress, but a story far from over. Physica D: Nonlinear Phenomena. 2015;306:48–81. https://doi.org/10.1016/j.physd.2015.05.003
13. de Reuille PB, Bohn-Courseau I, Ljung K, Morin H, Carraro N, Godin C, et al. Computer simulations reveal properties of the cell-cell signaling network at the shoot apex in *Arabidopsis*. Proc Natl Acad Sci USA. 2006;103(5):1627–1632. https://doi.org/10.1073/pnas.0510130103
14. Smith R, Guyomarc'h S, Mandel T, Reinhardt D, Kuhlemeier C, Prusinkiewicz P. A plausible model of phyllotaxis. Proc Natl Acad Sci USA. 2006;103(5):1301–1306. https://doi.org/10.1073/pnas.0510457103
15. Jönsson H, Heisler MG, Shapiro B, Meyerowitz E, Mjolsness E. An auxin-driven polarized transport model for phyllotaxis. Proc Natl Acad Sci USA. 2006;103(5):1633–1638. https://doi.org/10.1073/pnas.0509839103
16. Reinhardt D, Mandel T, Kuhlemeier C. Auxin regulates the initiation and radial position of plant lateral organs. Plant Cell. 2000;12(4):507–518. https://doi.org/10.1105/tpc.12.4.507
17. Reinhardt D, Frenz M, Mandel T, Kuhlemeier C. Microsurgical and laser ablation analysis of interactions between the zones and layers of the tomato shoot apical meristem. Development. 2003;130(17):4073–4083. https://doi.org/10.1242/dev.00596
18. Hofmeister W. Allgemeine Morphologie der Gewächse. In: du Bary A, Irmisch TH, Sachs J, editors. Handbuch der Physiologischen Botanik. Leipzig: Engelman; 1868. p. 405–664.
19. Snow M, Snow R. Experiments on phyllotaxis. II. The effect of displacing a primordium. Philos Trans R Soc Lond B. 1932;222:353–400. https://doi.org/10.1098/rstb.1932.0019
20. Reinhardt D, Pesce E, Stieger P, Mandel T, Baltensperger K, Bennett M, et al. Regulation of phyllotaxis by polar auxin transport. Nature. 2003;426(6964):255–260. https://doi.org/10.1038/nature02081
21. Rueda-Contreras MD, Aragón JL. Alan turing's chemical theory of phyllotaxis. Revista Mexicana de Física E. 2004;60(1):1–12.
22. Hotton S, Johnson V, Wilbarger J, Zwieniecki K, Atela P, Golé C, et al. The possible and the actual in phyllotaxis: bridging the gap between empirical observations and iterative models. J Plant Growth Regul. 2006;25:313–323. https://doi.org/10.1007/s00344-006-0067-9
23. Golé C, Dumais J, Douady S. Fibonacci or quasi-symmetric. Part II: botanical observations? Acta Soc Bot Pol. 2016;85(4):3534. https://doi.org/10.5586/asbp.3534

24. Mitchison GJ. Phyllotaxis and the Fibonacci series. Science. 1977;196(4287):270–275. https://doi.org/10.1126/science.196.4287.270
25. Douady S, Couder Y. Phyllotaxis as a self organizing iterative process, Part II: the spontaneous formation of a periodicity and the coexistence of spiral and whorled patterns J Theor Biol. 1996;178:275–294. https://doi.org/10.1006/jtbi.1996.0025
26. A Weisse. Sketch of the mechanical hypothesis of leaf-position. In: K. Goebel's Organography of plants. I. Oxford: Clarendon Press; 1900. p. 74–84.
27. Snow M, Snow R. Minimum areas and leaf determination. Proc R Soc Lond B Biol Sci. 1952;139(897):545–566. https://doi.org/10.1098/rspb.1952.0034
28. Couder Y. Initial transitions, order and disorder in phyllotactic patterns: the ontogeny of *Helianthus annuus*, a case study. Acta Soc Bot Pol. 1998;67:129–150. https://doi.org/10.5586/asbp.1998.016
29. Douady S, Couder Y. Phyllotaxis as a dynamical self organizing process Part I. J Theor Biol. 1996;178:255–274. https://doi.org/10.1006/jtbi.1996.0024
30. Zagórska-Marek B. Phyllotaxis triangular unit; phyllotactic transitions as the consequences of the apical wedge disclinations in a crystal-like pattern of the units. Acta Soc Bot Pol. 1987;56(2):229–255. https://doi.org/10.5586/asbp.1987.024
31. Bravais L, Bravais A. Essai sur la disposition des feuilles curvisériées. Annales des Sciences Naturelles. Botanique. 1837;7:42–110.
32. Bravais A. Mémoire sur les systèmes formés par des points distribués régulièrement sur un plan ou dans l'espace. Journal de l'École Polytechnique. 1850;19:1–128.
33. Douady S, Couder Y. Phyllotaxis as a physical self-organized growth process. Phys Rev Lett. 1992;68:2098–2101. https://doi.org/10.1103/PhysRevLett.68.2098
34. Atela P, Golé C, Hotton S. A dynamical system for plant pattern formation: a rigorous analysis. Journal of Nonlinear Science. 2002;12:641–676. https://doi.org/10.1007/s00332-002-0513-1
35. Adler I. A model of contact pressure in phyllotaxis. J Theor Biol. 1974;45:1–79. https://doi.org/10.1016/0022-5193(74)90043-5
36. Freeman E. Cylinder lattice applet. GeoGebra [Internet]. 2016 [cited 2016 Dec 31]. Available from: https://ggbm.at/NeHVks33
37. Mirabet V, Besnard F, Vernoux T, Boudaoud A. Noise and robustness in phyllotaxis. PLoS Comput Biol. 2012;8(2):e1002389. https://doi.org/10.1371/journal.pcbi.1002389
38. Douady S, Couder Y. Phyllotaxis as a dynamical self organizing process Part III: the simulation of the transient regimes of ontogeny. J Theor Biol. 1996;178:295–312. https://doi.org/10.1006/jtbi.1996.0026
39. Guédon Y, Refahi Y, Besnard F, Godin C, Vernoux, T. Pattern identification and characterization reveal permutations of organs as a key genetically controlled property of post-meristematic phyllotaxis, J Theor Biol. 2013;338:94–110. https://doi.org/10.1016/j.jtbi.2013.07.026
40. Bachmann K. Evolutionary genetics and the genetic control of morphogenesis in flowering plants. In: Evolutionary biology. Boston, MA: Springer; 1983. p. 157–208. https://doi.org/10.1007/978-1-4615-6971-8_5
41. Fredeen A, Horning J, Madill R. Spiral phyllotaxis of needle fascicles on branches and scales on cones in *Pinus contorta* var. *latifolia*: are they influenced by wood-grain spiral? Can J Bot. 2002;80(2):166–175. https://doi.org/10.1139/b02-002
42. Prusinkiewicz P. Graphical applications of L-systems. In: Green M, editor. Proceedings of Graphics Interface and Vision Interface. Vol. 86; 1986 May 26–30; Vancouver, Canada. Toronto, ON: Canadian Information Processing Society; 1986. p. 247–253. https://doi.org/10.20380/GI1986.44
43. Kunz M. Phyllotaxie, billards polygonaux et thorie des nombres [PhD thesis]. Lausanne: Université de Lausanne, Switzerland; 1997.
44. Fenichel N. Persistence and smoothness of invariant manifolds for flows. Indiana University Mathematics Journal. 1971;21(3):193–226. https://doi.org/10.1512/iumj.1972.21.21017
45. Levitov LS. Phyllotaxis of flux lattices in layered superconductors. Phys Rev Lett. 1991;66(2):224– 227. https://doi.org/10.1103/PhysRevLett.66.224